The Magnetocaloric Effect and Magnetic Refrigeration Near Room Temperature: Materials and Models

V. Franco, J.S. Blázquez, B. Ingale, and A. Conde

Departamento Física de la Materia Condensada, ICMSE-CSIC, Universidad de Sevilla, 41080 Sevilla, Spain; email: vfranco@us.es, jsebas@us.es, bingale@us.es, conde@us.es

Annu. Rev. Mater. Res. 2012. 42:305–42

First published online as a Review in Advance on May 29, 2012

The *Annual Review of Materials Research* is online at matsci.annualreviews.org

This article's doi: 10.1146/annurev-matsci-062910-100356

1531-7331/12/0804-0305$20.00

Keywords

magnetic entropy, adiabatic demagnetization, phase transition, equation of state

Abstract

In the past 20 years, there has been a surge in research on the magnetocaloric response of materials, due mainly to the possibility of applying this effect for magnetic refrigeration close to room temperature. This review is devoted to the main families of materials suitable for this application and to the procedures proposed to predict their response. Apart from the possible technological applications, we also discuss the use of magnetocaloric characterization to gain fundamental insight into the nature of the underlying phase transition.

1. INTRODUCTION

Magnetocaloric effect (MCE): the reversible temperature change of a magnetic material when magnetized or demagnetized

Magnetocaloric material (MCM): a magnetic material that exhibits a remarkable magnetocaloric effect

The magnetocaloric effect (MCE) is the reversible temperature change of a magnetic material upon the application or removal of a magnetic field. Its discovery is attributed to Warburg in 1881 (1), and it has been employed for achieving ultralow temperatures in research laboratories for decades. Indeed, its use led to the Nobel Prize in Chemistry being awarded to Giauque in 1949. In recent years, our society has become more energy conscious. To cut our energy use and be less dependent on limited resources, it is important to conduct research not only on renewable energies but also on technologies that would reduce energy consumption. We cannot forget that, regardless of its source, all energy production and transformation leave a footprint on the environment. Each country's energy situation is different, but let us take the United States as an example to calculate the relative importance of the four different end-use sectors of energy consumption (2). The combination of residential and commercial sectors (the latter of which includes buildings such as offices, malls, stores, schools, hospitals, hotels, warehouses, restaurants, places of worship, and more) accounts for 42% of total consumption. Consumption related to temperature control alone (space heating, cooling, and refrigeration) accounts for 50% of the energy consumption in homes (2005 data) and 57% in commercial buildings (2003 data). Consequently, increasing the energy efficiency of refrigeration systems would have a noticeable effect on energy bills. Magnetic refrigeration is a good candidate for making this improvement, as it is more energetically efficient than the process based on the compression/expansion of gases (magnetic refrigerator prototypes can achieve 60% of ideal (Carnot) efficiency, whereas the best commercial conventional refrigerator units can reach only 40%). Moreover, as no refrigerant gases are required for magnetic refrigeration, there is no concern about ozone depletion or greenhouse effect, which contributes further to its environmental friendliness.

For a simplistic explanation of a typical magnetic refrigeration cycle, we can separate a magnetocaloric material (MCM) into two subsystems: the magnetic moments and the lattice (**Figure 1**). At a finite temperature and in the absence of an external magnetic field, the orientation of the magnetic moments fluctuates and the lattice vibrates in a certain manner on the basis of the MCM's temperature (**Figure 2**; **Supplemental Video 1**—follow the **Supplemental Material link** from the Annual Reviews home page at **http://www.annualreviews.org**). When an external magnetic field is applied, the magnetic moments orient parallel to that field, decreasing the entropy associated with the magnetic subsystem. If the magnetization process is performed adiabatically, the decrease in magnetic entropy is compensated by an increase in lattice entropy, causing an increase in the temperature of the sample. At that stage, a heat transfer fluid (e.g., water if we are close to room temperature) can be employed to cool the MCM back to its initial

Supplemental Material

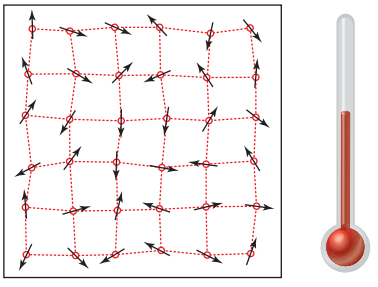

Figure 1

Magnetic and lattice subsystems in a magnetocaloric material.

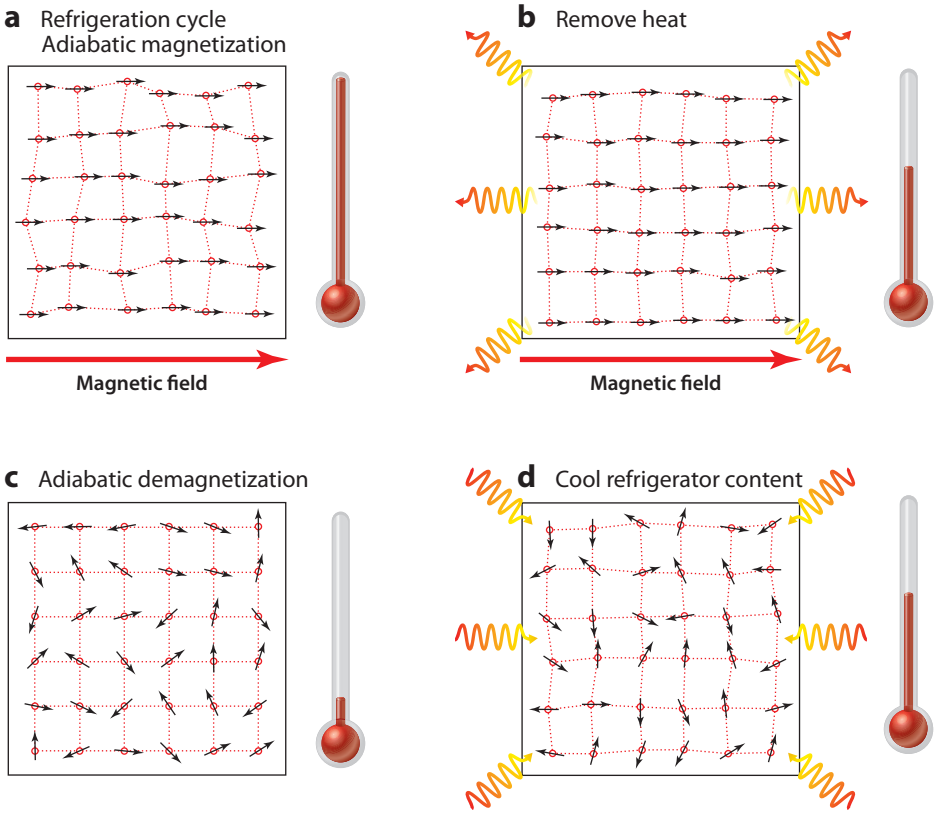

Figure 2

The four stages of a magnetic refrigeration cycle: (*a*) adiabatic magnetization, (*b*) remove heat, (*c*) adiabatic demagnetization, and (*d*) cool refrigerator contents.

temperature. Afterwards, an adiabatic demagnetization process occurs, increasing the magnetic entropy of the sample and, therefore, decreasing its lattice entropy and temperature. To cool the contents of the refrigerator, heat is extracted by passing a heat transfer fluid through the MCM. By performing these four steps cyclically, we are able to construct a magnetic refrigerator.

Up until very recently, research groups worldwide were developing magnetic refrigerators of different kinds (3–6), focusing mainly on demonstrating that it was a feasible technology and testing the performance of the devices with different magnetic refrigerants, with little concern (if any) about the characteristics that a device should have to be a realistic alternative to conventional refrigerators. However, this situation is changing, and papers linking device design parameters (and performance of magnetic refrigerators) to the cost of cooling are beginning to appear (7).

To characterize a MCM, there are several relevant magnitudes that should be measured. The most intuitive one is the adiabatic temperature change, ΔT_{ad}, which is the temperature change of the material when adiabatically magnetized/demagnetized. Less straightforward, but easier to determine (see the section below on experimental methods) is the magnetic entropy change, ΔS_M. As temperature changes are due to changes in the order of magnetic moments, it is natural that materials with large ΔS_M would be good candidates for magnetic refrigerants. Both magnitudes

are related to the temperature change of magnetization, M, and specific heat, c_p:

$$\Delta T_{ad} = -\mu_0 \int_0^{H_{\max}} \frac{T}{c_p} \left(\frac{\partial M}{\partial T}\right)_H dH, \quad 1.$$

and

$$\Delta S_M = \mu_0 \int_0^{H_{\max}} \left(\frac{\partial M}{\partial T}\right)_H dH, \quad 2.$$

where μ_0 is the permeability of free space and H_{max} is the maximum applied field. Usually c_p is approximated in the literature as field independent and, therefore, Equation 1 is replaced by

$$\Delta T_{ad} \approx -\frac{T \Delta S_M}{c_p}. \quad 3.$$

The validity of this relationship can be inferred by observing the typical shape of the $c_p(T)$ curves at different applied magnetic fields. Whichever is the order of the phase transition, there is a negligible influence of H on c_p for temperatures far from the transition temperature, which makes Equation 3 applicable in those cases. However, for those temperature ranges, the magnitude of the magnetocaloric effect is small, and therefore its characterization is of little interest. Close to the transition temperature, the behavior is different, depending on the order of the phase transition. For second-order magnetic phase transitions (SOPTs), c_p shows a discontinuity at the transition temperature, which is smeared out by the applied field (8). For first-order magnetic phase transitions (FOPTs), c_p exhibits a divergence at the transition temperature; either this divergence is strongly smeared out by the application of field, like for $DyCo_2$ (9), or the c_p peak is shifted to different temperatures by the application of H, like for LaFeSi, Mn(Fe,Co)As, MnCoGe, or GdSiGe (10). Therefore, the effect of applied field on c_p is larger for FOPTs. As a consequence, Equation 3 can be considered approximately valid for SOPT materials but not appropriate for FOPT materials.

Another relevant magnitude for evaluating the performance of a MCM is the amount of heat that can be transferred between its cold and hot reservoirs, which is referred to as refrigerant capacity, RC (or relative cooling power, RCP, by other authors):

$$RC(H) = \int_{T_{cold}}^{T_{bot}} \Delta S_M(T, H)\, dT, \quad 4.$$

where T_{cold} and T_{bot} are the temperatures of those reservoirs. Usually, these temperatures are viewed as corresponding to their full width at half maximum (FWHM) of the peak. Depending on the procedure used to calculate the integral, different definitions of RC appear: RC_{FWHM} approximates the integral by the product of the peak entropy change, ΔS_M^{pk}, and the full temperature width at half maximum of the peak, δT_{FWHM}; RC_{Area} corresponds to the calculation of the area under the $\Delta S_M(T)$ curve using the temperatures of the FWHM as the limits of integration; and RC_{WP} corresponds to the area of the largest rectangle that can be inscribed under the curve (11). As our goal is to use the material for cooling, before comparing the RC of different materials, we should subtract the energy losses that cause the material to heat up, such as hysteresis losses (12).

According to Equation 2, the largest MCE occurs at temperatures where the changes in magnetization are most abrupt. In the case of cryogenic refrigeration, in the sub-Kelvin range, the materials employed are paramagnetic salts, due to the divergence of their magnetic susceptibility at 0 K. However, if our goal is to apply this effect for temperature control close to room temperature, we need to find materials with a phase transition (and therefore an abrupt change of M) close to room temperature. This brings us to the simplest classification of MCMs: those with a FOPT (which, in many cases, is not only magnetic but magnetostructural) versus those with a SOPT. The former give rise to giant MCE (GMCE) (13), with large ΔT_{ad} and ΔS_M peaks. However,

First-order phase transition (FOPT): a phase transition that involves a discontinuity in the first derivative of free energy with respect to a thermodynamic variable

Second-order phase transition (SOPT): a phase transition with continuous first derivatives of free energy but discontinuous second derivatives and for which a description based on critical exponents is possible (also known as continuous phase transition)

Refrigerant capacity (RC): the amount of heat transferred between the hot and cold reservoirs, calculated as the temperature integral of the magnetic entropy change [also known as relative cooling power (RCP)]

the width of these peaks is not very broad, and this limits the applicability of the materials for a cyclic operation (14) unless they are used in stages. Additional problems include the thermal and magnetic hysteresis associated with FOPTs, which imply a waste of energy that could be used for cooling. However, notable examples in the literature attempt to minimize these problems (15). It should also be mentioned that large fields are usually needed to trigger the magnetostructural transitions, which is a drawback for the possible application of these materials under fields applied by a set of permanent magnets (in the 1.5–2 T range). Materials with a SOPT do not exhibit such large peaks, but their *RC* values can be larger than those for FOPT materials due to the broader nature of their transition. Thus, on the basis of the lack of thermal hysteresis and the possibility of reducing magnetic hysteresis by properly selecting the compositions, SOPT materials are now commonly used in magnetic refrigerator prototypes. There are reports indicating the use of FOPT materials in prototypes, but they are still less abundant. An interesting possibility is developing devices that allow the use of different kinds of materials inside the same prototype (16), which may accommodate both FOPT and SOPT materials.

The identification of promising magnetic refrigerant materials by comparing ΔS_M^{pk}, ΔT_{ad}^{pk}, and *RC* is somewhat different than identifying the best MCM to use in a prototype. The latter includes calculating the role of the coefficient of performance of the actual device, and other properties of the material, including corrosion resistance, mechanical properties, eddy current losses (and therefore the electrical resistivity of the material). The former identification can be made by physicists and materials scientists, whereas for the latter process, input from engineers designing the devices is crucial.

The relationship between material's properties and refrigerator performance is not straightforward, as additional parameters of the refrigerator design would affect the performance of the device. For example, in multistage refrigerators, for which several transitions are used and the operation of the different stages is narrowly focused around the peak of the ΔS_M (T) curve, RC may not be a proper metric to predict the total cooling power of the device. In any case, the selections of materials using large values of the abovementioned magnitudes would, in general, lead to a better chance of increasing the performance of the refrigerators.

Readers interested in the design and modeling of magnetic refrigerators are referred to other papers (4, 7, 17), as our focus is on materials properties rather than on the devices that apply them.

Currently, there are several possible applications of the MCE, including magnetic refrigeration close to room temperature (3), energy harvesting through thermomagnetic transitions (18), and the development of microfluidic pumps (19) and other thermomagnetic generators (20). Very recently, the oscillating MCE of diamagnetic materials has been proposed as a highly sensible magnetic field sensor (with a huge magnetic field in the background) (21). But interest in studying the MCE does not lie only with practical applications; before the hype triggered by such promising applications, the MCE was also studied to gain insight into the characteristics of phase transitions (22–26).

In this review, we focus our attention on certain materials that can be used for magnetic refrigeration and on models that can describe these materials' behavior. As there have been excellent reviews on the MCE in previous years (27–31), we, in many cases, rely on them for describing select materials properties. In that way, we are able to cover some of the topics that are not addressed in those reviews, such as the use of MCE studies to analyze the physics of phase transitions and the possibility of using emerging families of MCMs, including amorphous alloys, nanostructures, and composites. For the sake of completeness, however, some overlap is necessary. At the turn of the century, another review on MCMs (27) already included a section on amorphous alloys. The situation at that time was somewhat different, as there were roughly 15 papers in the scientific databases that dealt with this topic; through 2011, there was an increase of one order of magnitude in published results. Indeed, in 2006, there was a leap in the number of papers published

on amorphous MCMs, far surpassing the usual 1–3 papers per year, with 12 papers published in that year alone. Since then, the number of published studies on this kind of MCMs has been steadily increasing.

2. MEASUREMENT OF THE MAGNETOCALORIC EFFECT

2.1. Direct Measurements

Conceptually, the most straightforward procedure for characterizing a MCM is to adiabatically isolate a sample, place a temperature sensor on it, and record the temperature change of the sample when the magnetic field is swept. In this way, $\Delta T_{ad}(H)$ curves would be recorded as a function of the material's starting temperature (32–34). However, it is common practice to employ a differential thermocouple configuration, with one joint in contact with the sample and the other in contact with a massive nonmagnetic block at the bath temperature. Should rapid variations in magnetic field occur, parasitic electromotive force induced in the thermocouple wires must be counterbalanced to avoid spurious results (32).

This technique is appropriate when the thermal mass of the sample is much larger than the thermal mass of the sampleholder. Otherwise, as in the case of amorphous ribbons, recalibration procedures are necessary for estimating the actual response of the material (35).

2.2. Indirect Measurements

Indirect measurements of the MCE are much simpler to perform, as they use readily available experimental devices, such as magnetometers and calorimeters.

Perhaps the most common indirect characterization technique is to measure the temperature- and field-dependent magnetization curves and then use Equation 2 to calculate ΔS_M. Magnetization measurements are especially suitable for characterizing the MCE of samples with small mass. Recently, Peltier cell calorimeters for the determination of ΔS_M have also been developed (36).

A possible alternative is to measure the temperature dependence of the specific heat for different values of the applied field. By considering that the definition of the entropy is

$$S(T, H) = \int_0^T \frac{c_{p,H}}{T} dT, \qquad 5.$$

isofield curves of S as a function of T can be obtained. The magnetic entropy change can be calculated as the isothermal difference between two isofield curves, and the adiabatic temperature change can be calculated as the isentropic difference. Problems can arise from the extrapolation of the specific heat data to zero temperature, which is necessary to apply Equation 5. A comparison of the results provided by the different measurement procedures can be found in Reference 8.

Although Equation 2, which is the integral version of one of the Maxwell relations, is extremely helpful in calculating the magnetic entropy change of MCMs using simple magnetic measurements, its limitations should be considered before applying it. Otherwise, spurious results may occur, with calculated $|\Delta S_M^{pk}|$ values one order of magnitude larger than the actual values. The problem lies in the intrinsic difference between FOPTs and SOPTs. In the latter case, there is a continuous change from the low-temperature phase to the high-temperature phase, without there being a temperature range in which both phases coexist. FOPTs, however, involve a latent heat (absorbed or released without a change in temperature) and a coexistence of phases, which plays an important role in the calculation of the magnetic entropy change using Equation 2. For materials exhibiting SOPTs, such as Gd, when the values of temperature and magnetic field are given, the value of magnetization is unambiguously determined (taking into

account the moderately large fields used in magnetic refrigerators, we have disregarded magnetic hysteresis). But for FOPT materials, such as $Gd_5(SiGe)_4$ (37) or MnAs (38), there is a field-induced magnetic transition whose critical field depends on temperature and, therefore, the trajectory that we have followed along temperature and magnetic field affects the final state of the material. When ΔS_M is calculated from isothermal magnetic measurements, a spike appears. This has been interpreted to be caused by superheating of the ferromagnetic state when the isothermal measurements are taken with increasing magnetic field and which persists even if the Clausius-Clapeyron equation is used instead of the Maxwell relation (39). When calorimetric measurements are used, the spurious peaks do not appear because calorimetric curves are measured by sweeping the temperature at a constant applied magnetic field. For systems with coexisting phases, even if it is mathematically equivalent to calculate the thermal derivative first and the integration in field afterward, or vice versa, from a physical point of view, acquiring the data as a set of isofield $M(T)$ curves is not the same as acquiring them as a set of isothermal $M(H)$ curves. This is because the state of the system will vary on the basis of the manner in which the final values of temperature and field are reached, due to the fact that the mixture of phases will be different (40). Alternative measurement paths have been proposed to avoid this phase coexistence and allow for use of Equation 2 to properly calculate ΔS_M (39–41). Reference 10 comprehensively studies the different artifacts that can appear when different measuring protocols are used. These artifacts depend on the value of the maximum applied field and the way in which T and H are swept.

2.3. Dynamic Magnetocaloric Effect

Although there are not many studies on the dependence of the MCE on the rate of variation of H, it is important to consider this aspect of the magnetocaloric response. In fact, because any magnetic refrigerator device operates under cyclic conditions, the higher the frequency that can be applied, the more heat that will be removed. Therefore, even if quasi-static characterization of a certain material (either with direct or indirect measurements) is important to establish its potential, the material's dynamic response may affect its final applicability.

Theoretical calculations (42) indicate that the maximum operation frequency of a magnetic refrigerator device is ~200 Hz, whereas current prototype units work in the range of a few cycles per second. Therefore, it is of the utmost importance to determine if an increase of the operation frequency will be deleterious for the performance of magnetic materials that are considered promising for magnetic refrigeration on the basis of their quasi-static properties.

Indirect measurements of MCE, taken either by magnetometry or by calorimetric methods, are intrinsically quasi-static. For small frequencies of operation (a few cycles per second), systems based on the direct measurement of ΔT_{ad} using thermocouples and with field applied by Halbach cylinders are appropriate (43). However, thermocouples have a time response that prevents an increase in operation frequency. An alternative solution (44), based on the method proposed by Levitin (45), consists of extracting ΔT_{ad} from a comparison of the temperature-dependent magnetization curves of a sample measured under isothermal conditions (in a conventional magnetometer) and under adiabatic conditions (in pulsed magnetic fields). In this way, ramp rates of the magnetic field equivalent to refrigerator frequencies of 25 Hz can be achieved.

3. MAGNETOCALORIC MATERIALS

3.1. Crystalline Materials Containing Rare Earth Metals

In this and the following section, crystalline materials are considered. This section is devoted to materials that contain rare earth (RE) elements, whereas the next describes the MCE of RE-free

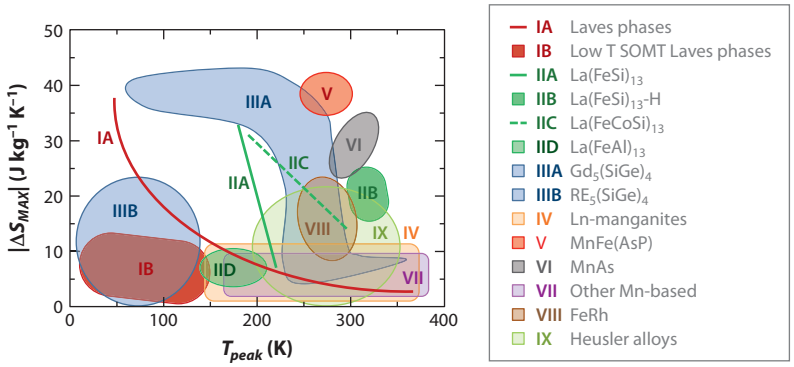

Figure 3

Maximum magnetic entropy change for $\Delta H = 5$ T versus peak temperature for different families of magnetocaloric materials.

Supplemental Material

systems. In both sections, crystalline systems are grouped into different families depending on the crystalline structure(s) exhibited near the transition temperature. **Figure 3** shows the relationship between the absolute value of the maximum magnetic entropy change and the transition temperature for the main families obtained for $\Delta H = 5$ T. Detailed data points and corresponding references can be found in **Supplemental Table 1**, which summarizes relevant MCE parameters for select crystalline compositions.

Gschneidner & Pecharsky (27) reviewed the magnetocaloric behavior of pure lanthanide elements in 2000. However, we should mention some recent results on the strong enhancement of MCE for low field changes in ultrathin layers when their thickness is below the helix period and thus no helical magnetic order (typically found in RE metals) is formed. In the case of *c*-axis-oriented Ho ultrathin film, the MCE curve displayed a caret-like shape, as typically found for conventional ferromagnets (27), with a Curie temperature, $T_C = 121$ K, and ΔT_{ad} was enhanced by an order of magnitude with respect to bulk samples ($\Delta T_{ad} = 1.3$ K and 0.08 K for $\Delta H = 0.2$ T for thin film and bulk samples, respectively) (46).

In this section, alloys containing RE metals are considered in the following sequence: Laves phases, $La(Fe,Si)_{13}$ intermetallics and their derivatives, gadolinium germanium silicides (5:4 stoichiometry) and their derivatives, ferromagnetic lanthanum manganites, and other crystalline intermetallic compounds containing RE metals.

3.1.1. Laves phases. Laves phases, with stoichiometry A-B_2, crystallize in three types of structures: cubic $MgCu_2$-type, hexagonal $MgZn_2$-type, and hexagonal $MgNi_2$-type structures. However, the intermetallic compounds of interest for MCE are the cubic phase, with A an RE metal (including Sc and Y) and B mainly a transition metal (TM) (other elements such as Al, Ga, and Ge can also be present).

In the cubic Laves phases (space group $Fd\bar{3}m$), RE atoms form a diamond lattice, whereas the other atoms surround the RE atoms forming tetrahedra. For those systems with TMs, two magnetic sublattices could appear: one formed by magnetic RE atoms and another formed by itinerant electron magnetism due to TMs. In the case of $RECo_2$ compounds, the two magnetic sublattices couple parallel for light RE elements (thus, Laves phases containing Pr, Nd, and Sm are ferromagnets) and couple antiparallel for heavy RE elements (thus, Laves phases containing Gd, Tb, Dy, Ho, and Er are ferrimagnets).

GMCE has been reported for Laves phases for which an itinerant electron metamagnetic transition occurs, similar to that observed for $La(Fe,Si)_{13}$ compounds (see below). An itinerant metamagnetic transition describes a magnetic transition from a paramagnetic structure to an ordered structure of itinerant electrons induced by the application of a magnetic field (47). For Laves phases, the molecular field of RE is responsible for this transition. A review on this subject can be found in Reference 48. For these compounds, the magnetovolume effects play a very important role in determining the nature of the magnetic transition and the associated MCE. Khmelevskyi & Mohn (49) developed a model for $RECo_2$ compounds considering magnetovolume effects and spin fluctuations. In this model, the order of the magnetic transition is predicted from the lattice parameter: For lattice parameters above 0.722 nm, Co atoms carry a magnetic moment and therefore SOPT is expected, whereas for lattice parameters below 0.705 nm, Co has no magnetic moment. Itinerant electron metamagnetism (and thus FOPT) occurs for values in between those limits; at such values, the molecular field of the RE lattice can induce a magnetic moment in the 3d sublattice. Two exceptions, $TbCo_2$ and $TmCo_2$, both appearing in the binary $RECo_2$ series, undergo SOPT with lattice parameters of 0.721 nm and 0.714 nm, respectively. The former case is explained due to the high Curie temperature (>200 K) leading to spin fluctuation effects; the latter, with a Curie temperature of only 4 K, is assumed to have a very weak molecular field, too weak to induce metamagnetism in the Co sublattice. In further support of Khmelevskyi & Mohn's model, element substitutions (provided they do not overly weaken Co sublattice interactions) leading to an increase in the lattice parameter yield an increase in Curie temperature and a loss of the first-order character of the transition, whereas application of pressure results in a decrease in the transition temperature (48).

There is a general parabolic decrease in $|\Delta S_M|$ with the transition temperature for the Laves phases (represented by line IA in **Figure 3**). FOPT is observed for Laves phases with GMCE and transition temperatures below ~200 K, whereas SOPT is observed for $RECo_2$ systems with higher transition temperatures. Substitution of Co can lead to loss of the first-order character of the transition for compounds with low Curie temperatures (48).

The study of composite alloys within this family is of interest for application purposes, due to the broad temperature range covered by compositional tailoring. Several of the References cited in this review have successfully used Landau theory in the MCE analysis of their respective compounds.

Metamagnetic transition and thus GMCE can be preserved in hydrogen-added YFe_2. However, the compound's cubic structure is no longer observed after a lowering of symmetry of the parent cubic compound is induced by hydrogen (deuterium) order in some particular tetrahedral sites. Thus, $YFe_2(H_{1-y}D_y)_{4.2}$ crystallizes in a monoclinic structure below 340 K with a strong isotopic effect on its magnetic properties (50). $|\Delta S_M| > 10$ J kg^{-1} K^{-1} for $\Delta H = 5$ T between 90 and 110 K for $YFe_2D_{4.2}$ below the metamagnetic transition at 127 K.

Other examples of crystalline compounds containing RE metals with A-B_2 stoichiometry, for which relevant MCE results can be found in the literature, are: hexagonal AlB_2-type (space group P6/mmm), orthorhombic $CeCu_2$-type (space group Imma), and hexagonal Ni_2In-type (space group $P6_3/mmc$). More details can be found in **Supplemental Table 1**. Compounds with the latter structure exhibit larger $|\Delta S_M|$, albeit at low temperatures [e.g., Ho_2Co (51) and HoCoSi (52) with −11 and −30 J kg^{-1} K^{-1} at 85 and 7 K, respectively, for $\Delta H = 5$ T].

3.1.2. $La[Fe(Si,Al)]_{13}$ family. Shen et al. (30) recently published a literature review on MCE in these systems. The La-Fe binary phase diagram shows an immiscible system, in which no intermetallic compounds form. The addition of small amounts of Si or Al allows the formation of a ferromagnetic, face-centered-cubic $NaZn_{13}$-type structure (space group $Fm\bar{3}c$) containing 112

atoms per unit cell. This intermetallic compound exhibits very interesting magnetic behavior, with Hu et al. (53) reporting GMCE for $LaFe_{11.4}Si_{1.6}$ in 2001 ($|\Delta S_M|$ close to 20 J kg^{-1} K^{-1} at 210 K, and $RC_{FWHM} = 530$ J kg^{-1} for $\Delta H = 5$ T). This was ascribed to a first-order itinerant electron metamagnetic transition, where a volume change of approximately 1% does not change the crystal symmetry. The itinerant electron metamagnetic transition can be lost due to compositional effects, leading to SOPT (29), which reduces MCE but implies negligible hysteresis losses.

Tuning the temperature transition either by changing the Fe/Si ratio or substituting a different RE metal for La yielded an almost linear relationship between ΔS_M and T_C (see line IIA in **Figure 3**). Moreover, the FOPT changed to a SOPT as temperature increased (30). A more efficient way to shift Curie temperature to higher temperatures, however, is by partial Co substitution for Fe (54) (see line IIC in **Figure 3**), as the magnetic moment of Fe is not seriously affected by Co substitution, but for $LaFe_{13-x}Si_x$ the average magnetic moment of Fe atoms decreases 0.286 μ_B per Si atom in the formula (30). Hydrides are also known to shift the temperature of the FOPT to higher values, without diminishing $|\Delta S_M|$ values, and with an enhancement of ΔT_{ad} as the heat capacity remains almost unchanged (30). However, hydrides in this compound are unstable above 423 K.

Single-phase $La(Fe,Si)_{13}$ alloys are very difficult to obtain and generally contain impurities, such as α-Fe phase (>5%) and other La-rich phases, even after prolonged annealing at high temperature (several days at approximately 1,273 K). These impurities must be factored into any comparison of different results, as composition can be inhomogeneous, and thus multiphase, rather than single-phase, behavior should be expected. To optimize homogeneity in the samples produced, melt-spinning technique has been used (55, 56), leading to a $NaZn_{13}$-type structure after 1 h annealing at 1,273 K with a significant reduction in magnetic and thermal hysteresis obtained in bulk alloys after a long time of annealing. Homogenization has also been improved by using reactive milling (57).

The use of Al instead of Si to stabilize the $NaZn_{13}$-type structure is less effective with respect to MCE signal (30). However, it is worth mentioning that $La(Fe_{0.98}Co_{0.02})_{11.7}Al_{1.3}$ was the first reported alloy of the family (58), exhibiting a SOPT with $\Delta S_M = -11$ J kg^{-1} K^{-1} and $T_C = 200$ K for $\Delta H = 5$ T, which compare positively with Gd results.

3.1.3. $Gd_5(Si,Ge)_4$ family. These systems, which exhibit GMCE and belong to the RE_5X_4 family, experience a magnetostructural FOPT between two polymorphic structures: orthorhombic Gd_5Si_4-type or Sm_5Ge_4-type structures (space group Pnma), which are the parent structures present in both binary Gd_5Si_4 and Gd_5Ge_4 compounds, and monoclinic structures (space group $P2_1/a$), which exist in a Si content range of $0.24 < x < 0.5$ in the pseudobinary $Gd_5(Si_xGe_{1-x})_4$ system (9). Three temperatures should be considered: the Curie temperatures of the monoclinic, $T_C{}^M$, and orthorhombic, $T_C{}^O$, phases and the critical temperature at which the free energies are equal in the orthorhombic and monoclinic phases, T_E. With the relationship $T_C{}^M < T_E < T_C{}^O$, the FOPT causes a sharp change in the magnetization and a GMCE, which is enhanced as the difference between $T_C{}^O$ and T_E increases.

In the magnetic phase diagram of the pseudobinary $Gd_5(Si_xGe_{1-x})_4$ system, the Ge-free compound is a simple ferromagnet with a Curie temperature of 335 K. As Ge content increases, Curie temperature linearly decreases to 295 K for $x \sim 0.5$. At this critical concentration, a monoclinic distortion in the parent orthorhombic Gd_5Si_4 structure leads to a different and more complex magnetic behavior: As temperature decreases, initially it orders ferromagnetically, but with low net magnetic moment and at lower temperatures, a FOPT occurs to another ferromagnetic phase. Both transition temperatures decrease with Si content more rapidly than the T_C for alloys with $x > 0.5$. For compositions below $x = 0.24$, the monoclinic structure changes again to an

orthorhombic arrangement, and the system becomes ferrimagnetic near 125 K. Further cooling leads to a FOPT from the ferrimagnetic to ferromagnetic state. The transition temperature ascribed to this transformation decreases as Si content decreases (59).

For MCE, the prototypical alloy of this family is $Gd_5Ge_2Si_2$, which was discovered by Pecharsky & Gschneidner in 1997 (13) with the following MCE parameters: $\Delta S_M = -18.5$ J kg^{-1} K^{-1} and $\Delta T_{ad} = 15$ K at 276 K and $\Delta H = 5$ T. The thermal hysteresis ~2–5 K was lower than that of the alloy FeRh, the only compound known to have GMCE at that time. Ge enrichment shifts the transition temperature to lower values but enhances MCE signal (59).

Compositional changes substituting different elements for Si and Ge generally destroy GMCE and shift the Curie temperature to higher values (~300 K). In the cases of Ga (60), Sn (61, 62), Mn (63), and In (64), however, GMCE is preserved.

Hysteresis losses are strongly reduced after 0.1 addition per formula unit of Cu, Ga, Mn, and Al (60), as was noted above for Fe (12). In the case of Fe, this reduction is more pronounced with Ge substitution than Si substitution in $Gd_5Ge_2Si_2$ (hysteresis losses are almost zero for $Gd_5Ge_{1.75}Si_2Fe_{0.25}$) (65).

Recent results (66) show that partial substitution of Nb in $Gd_5Si_{2-x}Ge_{2-x}Nb_{2x}$ alloys increased Curie temperature and MCE signal as x increased to x = 0.05 (T_C~ 295 K and $\Delta S_M = -9.6$ J kg^{-1} K^{-1} for $\Delta H = 2$ T, ~50% enhancement over the Nb-free alloy). Moreover, in this case, a lower amount of detrimental Gd_5Si_3 phase has been found.

Some of the problems encountered in attempts to optimize this family are related to its inhomogeneity (presence of polymorphic orthorhombic phase) and impurity phases, such as hexagonal Gd_5Si_3 phase, which is antiferromagnetic and detrimental to MCE. To homogenize the alloy, high-temperature annealing is generally performed. A clear enhancement of ΔS_M and ΔT_{ad} has been reported for annealed samples as compared with arc-melted samples without postannealing. This enhancement has been ascribed both to a reordering of Ge and Si atoms in their corresponding sites within the monoclinic structure and to a removal of the retained polymorphic orthorhombic phase (67). A higher cooling rate from the arc melting also enhances MCE (68), as does the use of high-purity Gd instead of commercial grade (69).

In general, the substitution of other RE metals for Gd weakens MCE as shown in **Figure 3**. However, small partial substitution of Zr for Gd in $Gd_{5-x}Zr_xSi_2Ge_2$ alloys was recently proposed to reduce the amount of antiferromagnetic and detrimental hexagonal Gd_5Si_3-type phase (70). At small values of x (x = 0.05), the amount of preferred 5:4-type phase increased to 85% from 70% for x = 0. However, a higher amount of Zr yielded a reduced fraction of 5:4 phase. Moreover, the presence of Zr changed the 5:4 monoclinic structure exhibited by Zr-free alloys to a 5:4 orthorhombic one; thus, the FOPT changed to SOPT. Nevertheless, although $|\Delta S_M|$ for $\Delta H = 2$ T decreased from 7.8 to 5.5 J kg^{-1} K^{-1} when x was increased from 0 to 0.05, RC_{FWHM} was enhanced three times from ~50 to more than 150 J kg^{-1}. For compounds containing Zr, Curie temperature monotonically decreased from 292 to 272 K when x was increased from 0.05 to 0.20.

3.1.4. Ferromagnetic lanthanum manganites. Ferromagnetic lanthanum manganites were extensively reviewed by Phan & Yu in 2007 (71). For magnetocaloric purposes, these compounds are ferromagnetic perovskite manganites deriving from lanthanum manganite, $LaMnO_3$. However, this phase is semiconducting and has an antiferromagnetic order temperature of 150 K. Excess oxygen, La deficiency, or the substitution of a nontrivalent ion for a trivalent RE ion leads to appearance of mixed valence in Mn ions and to ferromagnetic coupling between Mn^{4+} and Mn^{3+} ions via double-exchange mechanisms.

This family of manganites exhibits quite complicated magnetic phase diagrams as a function of their composition. Almost all metallic manganites are ferromagnetic, as electron transfer

enhances the double-exchange mechanism, whereas in antiferromagnetic manganites antiparallel coupling between neighboring Mn ions leads to a zero value for the hopping integral and thus to an insulator system. However, the picture can get much more complicated with other types of magnetism exhibited by a wide variety of manganites in this family, such as antiferromagnetic insulators, ferromagnetic insulators, antiferromagnetic metals, glassy insulators, more complex canted magnetic structures, and mixed-phase states. The reason for such a broad phenomenology is the small difference between possible ground states due to competition among a number of different interactions, as listed in Reference 72: crystal field splitting between e_g and t_{2g} electrons, kinetic energy of e_g electrons, Hund coupling between e_g and t_{2g} electrons, Jahn-Teller character of Mn^{3+} ions, and Heisenberg magnetic coupling between nearest neighbors.

In the case of ferromagnetic manganites, Curie temperature can be tailored in a wide range (from ~150 to ~375 K) by substituting divalent ions (Ca^{2+}, Ba^{2+}, Sr^{2+}, Pb^{2+}, etc.) or monovalent ions (Na^{1+}, K^{1+}, Ag^{1+}, Li^{1+}, etc.) for La or by creating an excess of oxygen (see Reference 71 and references therein). The average radii of the cations at the different sites also affect the ground state of these manganites. This property can be tuned by partial substitution of La^{3+} with another trivalent RE ion, Y^{3+} or Bi^{3+}, or in La-free Pr or Nd manganites (71). A characteristic parameter used to describe the manganite behavior is the ionic size tolerance factor, defined as:

$$t = \frac{<R_{La}> + R_O}{\sqrt{2}(<R_{Mn}> + R_O)},$$

where $<R_{La}>$ is the average radius of La-site atoms, $<R_{Mn}>$ is the average radius of Mn-site atoms, and R_O is the radius of the O^{2-} ion. Curie temperature increases with the tolerance factor and saturates ($T_C \sim 300$ K) at $t > 0.905$.

Another possible method for tailoring T_C is via substitution of Mn with another TM or a semimetal/metaloid. This generally leads to a deterioration of ferromagnetic character (decreasing Curie temperature), as the ferromagnetic double-exchange mechanism in Mn^{3+}-O^{2-}-Mn^{4+} groups competes with an antiferromagnetic superexchange mechanism when Mn is substituted with another TM.

The first studies on MCE of manganites appeared in 1996 (73, 74); to date, there is no clear correlation, for these compounds, of ΔS_M (or RC_{FWHM}) with the tolerance factor and thus with T_C. However, it is worth noting that nonstoichiometric systems likely affect their magnetic properties and could explain the dispersion of the reported data. Several factors apart from compositional changes affect MCE signal: grain size (75–77), chemical order (78–80), sintering temperature (81, 82), and pressure application (83).

3.1.5. Other crystalline compounds containing rare earth metals. Although intermetallic compounds crystallizing in a $ThCr_2Si_2$-type structure generally show a transition temperature well below room temperature, $La(Mn_{1-x}Fe_x)_2Ge_2$ alloys exhibit a Curie transition between 275 and 310 K as x decreases from 0.1 to 0.05, with a $|\Delta S_M| \sim 1$ J kg^{-1} K^{-1} for $\Delta H = 1.8$ T (84).

Recent studies have focused on intermetallics with RE_2X_{17} stoichiometry, which crystallize in two types of structures: rhombohedral Th_2Zn_{17}-type (space group $R\bar{3}m$) and hexagonal Th_2Ni_{17}-type (space group $P6_3/mmc$) structures. Ball-milled, nanometer-sized powders of Pr_2Fe_{17} preserving the Th_2Zn_{17}-type structure exhibited lower $|\Delta S_M|$ values than their bulk counterparts (85) (4.5 and 6.3 J kg^{-1} K^{-1} for $\Delta H = 5$ T, respectively) although RC increased as $\Delta S(T)$ curves became broader and T_C increased from ~290 to ~300 K (86). Some α-Fe impurities were found, but a Pr content above 12 at.% can be used to avoid their formation. For $Pr_{10+x}Fe_{90-x}$ alloy series, MCE was optimized in $Pr_{13}Fe_{87}$ alloys with the Pr_2Fe_{17} phase as the single-crystalline phase detected

(87). Pseudobinary $Ce_{2-x}RE_xFe_{17}$ compounds, with RE = Y (x = 1.2), Pr (x = 1.5), and Dy (x = 1.15), also crystallize in a Th_2Zn_{17}-type structure and have been studied with the aim of tuning SOPT temperature (253, 264, and 273 K for Y, Pr, and Dy compounds, respectively) (88). $|\Delta S_M|$ and RC values decreased in a Pr > Y > Dy order (5.3, 4.3, and 3.3 J kg^{-1} K^{-1}, respectively, for $\Delta H = 5$ T). The $Ce_2Fe_{17-x}Mn_x$ ($x \leq 2$) series also crystallizes in a Th_2Zn_{17}-type structure (89). These alloys exhibited two magnetic transitions for $0 \leq x \leq 0.35$ and $1.3 \leq x \leq 2$ compounds—a ferromagnetic to antiferromagnetic transition (decreasing as x increased from 0 to 0.35 from 94.4 to 22 K and increasing as x increased from 1.3 to 2 from 9 to 80 K) and an antiferromagnetic to paramagnetic transition—whereas a single Néel transition was observed for $0.5 \leq x \leq 1$ compounds. Due to the antiferromagnetic-paramagnetic transformation (with Néel temperature decreasing from 209 to 168 K as x increased from 0.35 to 2), low values of x yielded $\Delta S_M \sim -3$ J kg^{-1} K^{-1}, with absolute values decreasing to 50% for the x = 2 compound.

Y_2Fe_{17} crystallizes in a Th_2Ni_{17}-type structure with a Curie temperature of 295 K and $\Delta S_M \sim -5$ J kg^{-1} K^{-1} for $\Delta H = 5$ T (85). A higher Curie temperature of ~310 K was measured in ribbons produced by melt spinning with $\Delta S_M = -1.6$ J kg^{-1} K^{-1} for $\Delta H = 1$ T (90). Also crystallizing in a Th_2Ni_{17}-type structure, Er_2Ni_{17} was ferrimagnetic below 150 K, with a compensation temperature of 63 K for $H = 0.02$ T, shifting to lower values for higher fields. ΔS_M at the ferrimagnetic-paramagnetic transition was approximately −0.7 J kg^{-1} K^{-1} for $\Delta H = 5$ T, with inverse MCE near 60 K (91). The $Lu_2Fe_{17-x}Mn_x$ ($0 \leq x \leq 2$) series crystallizes in a Th_2Ni_{17}-type structure as well (some α-Fe impurities were also found) (92). Alloys with $x \leq 0.5$ exhibited a Néel temperature of ~278 K but changed to ferromagnetic state at lower temperature, which increased from 135 to 249 K as Mn content increased from 0 to 0.5 at%. Alloys with $0.7 \leq x \leq 2$ were ferromagnets with $T_C = 287$ K for x = 0.7. Maximum $|\Delta S_M|$ of 3.6 J kg^{-1} K^{-1} for $\Delta H = 5$ T was achieved for x = 0.7, where the FOPT and SOPT merged.

Gd_3TM [TM = Co, Ni (93), and Rh (94)] and Tb_3Co (95) crystallize in a orthorhombic cementite-like Fe_3C-type structure. Néel temperatures were 128 and 99 K for Gd_3Co and Gd_3Ni, with $\Delta S_M \sim -11$ and −5 J kg^{-1} K^{-1}, respectively, for $\Delta H = 5$ T. For Gd_3Rh, MCE peaked at 112 K ($\Delta S_M = -9.2$ J kg^{-1} K^{-1} for $\Delta H = 5$ T), close to the ordering temperature of, presumably, a canted antiferromagnetic system (94).

Hexagonal $Ce_6Ni_2Si_3$-type structure (space group $P6_3/m$) was exhibited in the $RE_6Co_2Si_3$ series where RE = Gd, with Curie temperature of 295 K, $\Delta S_M = -6.3$ J kg^{-1} K^{-1} for $\Delta H = 5$ T, and a broad $\Delta S(T)$ peak (FWHM >100 K and $RC_{FWHM} \sim 700$ J kg^{-1}) (96). Small changes in the stoichiometry to $RE_6Co_{1.67}Si_3$ retained the $Ce_6Ni_2Si_3$-type structure and SOPT.

Some boride compounds with transition temperatures above 150 K have also been studied. Metastable $NdFe_{12}B_6$ compound can be obtained from devitrification of amorphous alloys (aside from ~20% of α-Fe phase) and exhibits an abrupt change in magnetization near its Curie temperature of ~220 K, with $\Delta S_M = -8.4$ J kg^{-1} K^{-1} and $\Delta T_{ad} = 3.2$ K for $\Delta H = 1$ T (97). This intermetallic crystallizes in a hexagonal $SrNi_{12}B_6$-type (space group $R\bar{3}m$) structure, with a high magnetic moment of 19.7 μ_B per formula unit. Mösssbauer spectrometry results suggest that a FOPT from ferromagnetic to paramagnetic state is responsible for the high MCE parameters (98). The metastability of this compound can be overcome by alloying it with the isostructural compound $NdCo_{12}B_6$, which orders at 170 K. However, the first-order character of the transition is lost, leading to a moderate ΔS_M value (−1.4 J kg^{-1} K^{-1} for $\Delta H = 1$ T) that decreases with increasing Fe content. Nevertheless, RCs were almost constant along the series as the $\Delta S(T)$ curves became broader. Similar to the compound containing Nd, $PrFe_{12}B_6$ exhibited a FOPT at 200 K from ferromagnetic to paramagnetic state, accompanied by a lattice contraction leading to high MCE values (−11.7 J kg^{-1} K^{-1} for $\Delta H = 2$ T) (99).

3.2. Rare Earth–Free Crystalline Materials

The main reason for considering compounds containing Mn in the MCE study of transition-based compounds is the high magnetic moment of Mn atoms, which is the highest value among TMs (up to 4 μ_B in some intermetallics). A recent review by Brück et al. (84) focused on these systems. In the present section, we consider RE-free crystalline phases in the following order: Heusler alloys, Mn-TM-Si-Ge compounds, $(Mn,TM)_5X_3$ compounds, MnAs alloys, MnFePAs alloys, FeRh alloys, and other RE-free alloys.

3.2.1. Heusler alloys. Heusler alloys are ordered intermetallics with the generic formula X_2YZ (BiF_3-type structure) in which the three components occupy the crystallographically nonequivalent positions of the space group $Fm\bar{3}m$. X and Y are 3d elements, and Z is IIIA-VA group element. These alloys show magnetism due to the X and/or Y elements. Although they are metals, their magnetic properties can often be described in terms of localized magnetic moments with indirect exchange interactions. In a broad composition range, these alloys transform from a parent austenitic state ($L2_1$) to a product martensitic state (tetragonal or modulated 5M and 7M, where M refers to the monoclinicity resulting from the distortion associated with the modulation). The structural transformation in these Heusler alloys is first order with a narrow thermal hysteresis. The application of a magnetic field leads to a large MCE near this transformation, and the MCE reaches its maximum when the martensitic transformation (T_M) and the magnetic transition temperatures lie close to each other (100, 101).

The entropy change ΔS associated with the structural transition in a polycrystalline Ni-Mn-Ga alloy was first reported in 2000 by Hu et al. (100) with a positive entropy change (inverse effect) of 4.1 J kg^{-1} K^{-1} for $\Delta H < 1$ T. Further investigations reported a positive-to-negative crossover of the entropy change (i.e., conventional MCE) with a large value of ~ -18 J kg^{-1} K^{-1} ($T = 290$ K) for $\Delta H = 5$ T in a single crystal of $Ni_{52.6}Mn_{23.1}Ga_{24.3}$ (100). The inverse effect taking place at low fields was related to the strong uniaxial magnetocrystalline anisotropy of the martensitic phase. When the composition was varied in such a way that the martensitic transition temperature approached the Curie temperature, the anisotropy weakened with a corresponding decrease in the inverse contribution, and conventional behavior became dominant (102, 103). Since then, numerous investigations on the magnetic properties and MCE of various compositions of Ni-Mn-Ga ferromagnetic shape memory Heusler alloys have been carried out (29).

Recently, the Ga-free $Ni_{50}Mn_{50-y}Z_y$ (Z = In, Sn, or Sb) series of Heusler alloys were characterized by a sequence of magnetic [from paramagnetic (PM) to ferromagnetic (FM) to antiferromagnetic (AFM)] and structural (austenite-martensite) phase transitions close to room temperature. Direct MCE occurred in the SOPT region (PM-FM), whereas inverse MCE was observed at the FOPT martensitic transition and near the metamagnetic FM-AFM transition (merged metamagnetostructural transition).

In the $Ni_{50}Mn_{50-x}Sn_x$ (x = 13–15) series, an optimal ΔS_M of +18.0 J kg^{-1} K^{-1} for $\Delta H = 5$ T was reported by Krenke et al. (104). Very recently, Khovaylo et al. (105) studied the MCE of a Co-doped Ni-Mn-Sn alloy by direct and indirect methods and reported an apparent discrepancy between ΔS_M and ΔT_{ad}, which was due to the hysteretical behavior of the magnetostructural transition. The hysteresis caused the MCE to strongly depend on the temperature and field history of the experimental processes.

A large ΔS_M takes place near room temperature for these metamagnetic shape memory alloys, accompanied by a large thermal hysteresis, which may be as large as 20 K for Ni-Mn-Sn alloys (106) and 10 K for Ni-Co-Mn-In alloys (107). Future studies in this area may consider thermal processing and alloy composition, as both factors are known to influence the magnitude of the

hysteresis (108). Furthermore, the kinetics of the phase transformation process warrants further study, as either structural or magnetic relaxation processes may affect hysteresis widths. These alloys have also been studied by rapid solidification/melt spinning by Hernando et al. (109) and Babita et al. (110, 111) in a low field near 2 T to observe the effect on ΔS_M. A maximum positive ΔS_M of 35.8 J kg^{-1} K^{-1} at FOPT was achieved for a field change of 5 T in the alloy $Ni_{50}Mn_{35}In_{15}$ (112).

Reports on direct measurements of the field-induced ΔT_{ad} are scarce. Measurements of ΔT_{ad} have been conducted with a thermocouple in direct contact with the sample in Ni-Mn-Ga alloys with T_M and the magnetic transition temperature close to each other (113, 114). The temperature dependence of ΔT_{ad} is in qualitative agreement with that exhibited by ΔS_M, but the measured values are about one order of magnitude lower than those computed from entropy and specific heat data. For the Ni-Mn-In system, magnetization, specific heat, and direct temperature measurements were conducted on a series of isoelectronic Ga-doped Ni-Mn-In compounds (115). Recently, researchers observed the measurement of MCE in $Ni_{50}Mn_{37}Sn_{13}$ and $Ni_{40}Mn_{50}In_{10}$ ribbons by a method that used a modulated magnetic field (116) and reported both the direct and inverse MCE associated with magnetic and structural phase transitions.

3.2.2. Mn-TM-(Si,Ge) compounds. $MnFe_{1-x}Co_xGe$ compounds change from a hexagonal Ni_2In structure (space group $P6_3/mmc$) for $x < 0.8$ to an orthorhombic TiNiSi structure (space group Pnma) for $x > 0.85$ (117). Independent of the structure, a continuous increase in the Curie temperature from ~150 to ~350 K is observed as Co content increases (the maximum absolute entropy change in the series is 9 J kg^{-1} K^{-1} for a field change of 5 T with $T_C = 289$ K).

More recently, Trung et al. (44) discovered a GMCE near room temperature by introducing interstitial boron atoms in $MnCoGeB_x$ alloys. The structural and magnetic transitions in MnCoGe can be controlled to coincide, leading to a single first-order magneto-structural transition from two coexisting ferromagnetic TiNiSi- and Ni_2In-type phases to an almost single-phase paramagnetic Ni_2In-type structure. The optimum MCE data were obtained for $x = 0.02$: $\Delta S_M = -47.3$ J kg^{-1} K^{-1} for $\Delta H = 5$ T at $T = 287$ K, although the thermal hysteresis was 14 K.

Orthorhombic TiNiSi structure is also observed in $MnCoSi_{1-x}Ge_x$ alloys (118), which exhibit antiferromagnetic behavior at low fields, but ferromagnetic character can be induced by metamagnetic transition at moderate fields (above 1 T, e.g., accessible by using permanent FeNdB magnets). Inverse MCE was observed near 200 K and was ascribed to the fact that this metamagnetic transition ($\Delta S = +4$ J kg^{-1} K^{-1} for $\Delta H = 1$ T) was transition temperature field dependent. The thermal hysteresis and magnetic hysteresis (reported at 8 K and 0.35 T, respectively) were much lower than for other FOPT materials.

3.2.3. $(Mn,TM)_5X_3$ compounds. All these compounds crystallize in a hexagonal Mn_5Si_3-type structure (space group $P6_3/mcm$). In the $Mn_{5-x}Fe_xSi_3$ series (119), the highest absolute value of magnetic entropy change (~2 J kg^{-1} K^{-1}) for a field change of 2 T was observed for $x = 4$, for which the magnetic moments of transition elements were maxima (1.4 and 2.5 μ_B for 4d and 6g sites, respectively). Fe-rich alloys exhibited a ferromagnetic to paramagnetic transition close to room temperature, and Fe-poor compositions exhibited complex antiferromagnetic behaviors and orthorhombic distortions at temperatures so low as to be inapplicable for room temperature appliances. Some divergences concerning the magnetic character arose for $x = 3$.

A much higher absolute value [~9 J kg^{-1} K^{-1} for 5 T change, which is above 80% of that of Gd (120)] was achieved in the alloy Mn_5Ge_3, with a Curie temperature of 296 K and an average magnetic moment for the Mn atoms of 2.6 μ_B. Partial substitution of Sb (120) for Ge slightly increased T_C and yielded a decrease in the $|\Delta S_M|$ peak ascribed to a decrease in the average

magnetic moment, but the width of the magnetocaloric peak increased, which is interesting for enhancing RC.

A similar compound, Mn_5PB_2, which crystallizes in a tetragonal structure (space group I4/mcm), was recently reported to achieve $\Delta S_M \sim -5$ J kg^{-1} K^{-1} for $\Delta H = 5$ T at 302 K during its SOPT from ferromagnetic to paramagnetic state (121).

3.2.4. MnAs alloys. In this section, we include also those alloys based on previously discussed alloys containing arsenic. The poisonous nature of arsenic has led to a strong effort to develop arsenic-free alloys with the same outstanding MCE properties exhibited by these alloys and, therefore, also to preserve their crystal structures. Two families are considered here: on the one hand, the family derived from MnAs and, on the other hand, the so-called Fe_2P-type compounds.

MnAs exhibited a FOPT at 318 K from ferromagnetic hexagonal NiAs-type structure to paramagnetic orthorhombic MnP-type structure with huge magnetic entropy change (-30 J kg^{-1} K^{-1} for $\Delta H = 5$ T) but with large thermal hysteresis (6 K) that can be reduced by partial substitution of As for Sb (<1 K). At 378 K, a SOPT occurred, changing again from MnP type to NiAs type; the MnP-type structure was stable only in the thermal range from 318 to 378 K (38). Excess Mn in alloys with partial substitution of Sb for As (122) resulted in an apparent SOPT (although some NiAs-type structure remained), tuning the Curie temperature between 220 and 318 K and maintaining large values of MCE. The sharp transition found for alloys with little excess Mn is ascribed to a nonordinary itinerant electron metamagnetic transition (i.e., unlike for ordinary itinerant electron metamagnetic transition, field-induced transition disappeared under high pressure), whereas higher excess Mn yielded an ordinary SOPT. The nonordinary character is attributed to a strong decrease in magnetostriction at the Curie temperature. Recent work on the pressure dependence of magnetic properties of $MnAs_{1-x}Sb_x$ (123) observed a SOPT for $x > 3$, and that pressure destabilized the first-order character of the transition for $x = 3$.

Between 2004 and 2007, several papers reported on the so-called colossal MCE (magnetic entropy change above the theoretical magnetic limit) for MnAs at high pressure: for $\Delta H = 5$ T, $\Delta S_M = -40$ J kg^{-1} K^{-1} at atmospheric pressure, increasing with pressure up to -267 J kg^{-1} K^{-1} at 2.23 kbar. This was initially explained to be a result of magnetovolume coupling, although unrealistic Grüneissen parameters were necessary to fit the observed spikes in MCE (124). Recent theoretical results using Landau theory indicated that the so-called colossal MCE was just an artifact due to estimation of ΔS_M from nonequilibrium data without considering irreversibility or the mixed-phase regime typical of FOPTs (125).

Si-doping in $MnAs_{1-x}Si_x$ ($x \leq 0.09$) compounds (126) yielded a reduced thermal hysteresis (from 10 K for $x = 0.03$ to nearly zero for $x = 0.09$) as the magnetic transition changed from metamagnetic to SOPT. However, large values of $|\Delta S_M| > 10$ J kg^{-1} K^{-1} for $\Delta H = 5$ T were maintained. Interstitial nitrogen reduced Curie temperature and slightly enhanced MCE, and a virgin effect was observed (127); i.e., the first cooling process yielded a transition temperature different from those obtained after a second cooling.

3.2.5. MnFe(P,As) alloys. $MnFeP_{0.45}As_{0.55}$ was reported in 2002 to exhibit GMCE (128). The GMCE occurred as the magnetic and structural transformations coincided. $MnFeP_{1-x}As_x$ compounds crystallize in a hexagonal Fe_2P-type structure (space group $P\bar{6}2m$) for $0.15 < x < 0.66$. The Mn atoms occupy the 3g sites, and Fe, the 3f sites. However, P and As atoms are statistically distributed over the 2c and 1b sites. Changes in the As/P ratio enabled tuning of T_C between 200 and 350 K without losing the large MCE ($\Delta S_M = -15$ J kg^{-1} K^{-1} for $\Delta H = 2$ T). Thermal hysteresis, which is characteristic of such FOPTs, was less than 1 K (128). As Mn content increased

in the $Mn_{2-x}Fe_xP_{0.5}As_{0.5}$ series (129), the MCE peak shifted to lower temperatures and high $|\Delta S_M| > 15$ J kg^{-1} K^{-1} for $\Delta H = 2$ T were retained for $x \geq 0.8$.

Besides thermal hysteresis, which is inherent in a FOPT, another drawback to these alloys that contain arsenic is the poisonous nature of this element, which limits the use of such promising alloys for domestic appliances. Therefore, strong efforts have been focused in the substitution of Si and/or Ge for As. GMCE values were successfully preserved by combined substitution of Si and Ge for As in $MnFe(P_{0.89-x}Si_x)Ge_{0.11}$. However, thermal hysteresis strongly increased, above 15 K (130). Moreover, a virgin effect was observed, detecting a sharper transition temperature near 225 K when cooling the sample for the first time in comparison with subsequent heating and cooling cycles (about 275 K). Some authors ascribe this virgin effect to a pulverization of the sample during the first cooling. However, it is worth noting that virgin effects are well known to occur in FeRh compounds.

There is a strong, but not monotonic, dependency of T_C on Si content (130), which is ascribed to changes in the lattice parameters. Best results were obtained for $x = 0.26$, for which the lattice parameter ratio *a/c* was minimized ($T_C = 292$ K, $\Delta S_M = -16$ J kg^{-1} K^{-1} for $\Delta H = 2$ T). Recent results on B-doped $MnFeP_{0.63}Ge_{0.12}Si_{0.25}B_x$ show that increasing B content from $x = 0$ to $x = 0.03$ did not affect MCE, but T_C progressively increased from 300 to 347 K and thermal hysteresis decreased from 20 to 6 K (131).

The Fe_2P-type structure was also preserved for $MnFeP_{0.5}Ge_{0.5-x}Si_x$ compounds ($x = 0.1$ to 0.45) with T_C increasing from 300 to 548 K as x decreased from 0.45 to 0.1. Magnetic entropy change of those compounds with T_C close to room temperature was about -6 J kg^{-1} K^{-1} for $\Delta H = 1.5$ T (132).

For $MnFeP_{1-x}Si_x$ compounds (133), a hexagonal Fe_2P-type structure was observed for $0.28 < x < 0.64$, with a very large MCE for x close to 0.5 ($\Delta S = -30$ J kg^{-1} K^{-1} and $T_C = 300$ K for $\Delta H = 2$ T and $x = 0.5$). However, there was a large thermal hysteresis ascribed to the transition (above 20 K). An orthorhombic Co_2P-type structure was obtained for $x < 0.24$.

Even more promising results were obtained in recent years for the $Mn_{2-x}Fe_xP_{0.75}Ge_{0.25}$ series (134). In fact, although thermal hysteresis is a characteristic of FOPTs, it has been reduced by changing the Fe/Mn ratio in this series; the hysteresis was negligible for $y = 0.8$, where $\Delta S_M = -20$ J kg^{-1} K^{-1} for $\Delta H = 2$ T.

Impurity phases such as Mn_2O_3 and Fe_2MnSi have frequently been found during preparation of these compounds.

3.2.6. FeRh alloys. FeRh alloys (close to 1:1 stoichiometry) were the first system for which GMCE was reported (135). However, the lack of reproducibility of the initial results pointed to an irreversible character of GMCE in this system (136). This obstacle seems to be solved after Manekar & Roy (137) recently showed that, for a refrigeration cycle using this system, the first field increasing/decreasing cycle at hot temperature should be isothermal. Afterwards, an increase in adiabatic field could be carried out. The authors even suggested the possibility of there being a virgin $M(H)$ curve that causes the apparent irreversibility of the MCE in these alloys. The existence of a virgin effect is characteristic of other systems exhibiting a FOPT, as described above for the MnFe(P,Si,Ge) family (130).

The binary Fe-Rh phase diagram exhibits a ferromagnetic ordered CsCl-type structure (α' phase) for Rh content above 11% at 273 K and an ordered antiferromagnetic CsCl-type structure from ~49 to ~56% (α'' phase). FOPT, with a volume increase of 1%, can be induced thermally or by applying a magnetic field in this compositional range from antiferromagnetic α'' to ferromagnetic α' phase. The inverse MCE ascribed to this transition showed, for $Fe_{48}Rh_{52}$, $\Delta S_M \sim 12$ J kg^{-1} K^{-1} at $T \sim 300$ K and $RC_{FWHM} \sim 500$ J kg^{-1} for $\Delta H = 5$ T, although with a

large thermal hysteresis (137). The physical mechanism involved in this transition is controversial, but density functional theory calculations agree considering the crucial role of Rh moment on the stabilization of the ferromagnetic phase (138). In this phase, Fe atoms at the corner of a CsCl-type structure have a magnetic moment ~3 μ_B and Rh atoms at the center have a magnetic moment of ~1 μ_B. In the antiferromagnetic phase, Rh atoms have no magnetic moment.

Very recently, it was reported that small partial substitution of Ni for Fe in the alloy $Fe_{0.975}Ni_{0.025}Rh$ yielded an improvement of MCE above 50%. Although ΔS_M decreased to 9 J kg^{-1} K^{-1} at $T = 260$ K, the FWHM increased to 80 K for $\Delta H = 5$ T (139).

3.2.7. Other rare earth–free crystalline compounds. In Fe_xPt_{100-x} ($x = 78$–88) alloys (140), a phase transition occurs from the disordered FCC γ phase (higher temperatures) to the ordered BCC α phase (lower temperatures). This FOPT can also be induced by magnetic fields near the transition temperature. A GMCE ($\Delta S_M = -31.3$ J kg^{-1} K^{-1} for $\Delta H = 5$ T at ~250 K for $x = 79$) was ascribed to this transition and the associated and huge negative thermal expansion. A huge thermal hysteresis was also observed (30–40 K), which disappears for Fe content below 78% with the formation of Fe_3Pt phase.

Some nanocrystalline/nanosized spinel compounds have been studied in terms of their MCE reducing its Curie temperature and even appearing superparamagnetic behavior. Almost flat $\Delta S_M(T)$ curves (~0.25 J kg^{-1} K^{-1} for $\Delta H = 3$ T from 100 to 300 K) were obtained in ball-milled $ZnFe_2O_4$ (141), leading to $RC_{FWHM} > 75$ J kg^{-1} for $\Delta H = 3$ T. For nanosized $CoFe_2O_4$ deposited by the sol-gel technique, inverse MCE was reported (142), and unlike for the previously described ferrite, there was a peak in the $\Delta S_M(T)$ curve at 210 K of 0.25 J kg^{-1} K^{-1} for $\Delta H = 1.3$ T.

Cubic perovskite-type Mn_3GaC exhibited an inverse GMCE associated with an antiferromagnetic to ferromagnetic transition (FOPT) at 165 K, with $\Delta S_M = 15$ J kg^{-1} K^{-1} and $\Delta T_{ad} = 5.4$ K for $\Delta H = 2$ T (143). As field change increased, ΔS_M remained unchanged, but the curve broadened significantly (FWHM ~ 5 K for $\Delta H = 1$ T and ~ 25 K for $\Delta H = 5$ T). A SOPT from the ferromagnetic to paramagnetic state occurred where direct MCE was observed. In the $Mn_{3+x}Ga_xC$ series, Curie temperature increased from 250 K for $x = 0$ to 323.5 K for $x = 0.08$, whereas $|\Delta S_M|$ decreased from ~2.5 to below 1 J kg^{-1} K^{-1}. However, the width of the MCE peak broadened as x increased (144).

3.3. Amorphous Alloys

Maeda et al. (145) pioneered work in the area of amorphous alloys, analyzing the influence of alloying different metallic elements to the $(FeM)_{90}Zr_{10}$ alloy series. Belova & Stolyarov (146) continued those efforts, studying TM-based amorphous alloys of the FeCoSiB type. But shortly after that, the very few amorphous alloys that were studied as potential MCMs became dominated by RE-based alloys, with applicability at low temperatures (147).

The initial reason for keeping amorphous alloys outside of mainstream magnetocaloric research was the small peak value of ΔS_M (ΔS_M^{pk}) involved, when compared with the GMCMs (and also with respect to other SOPT materials). However, when the RC is taken into account, the comparison is more favorable (148–150). From an application point of view, TM-based amorphous alloys have additional characteristics that are desirable for magnetic refrigerants: low cost, higher electrical resistivity than crystalline materials (which minimizes eddy current losses), high corrosion resistance, tunability of the transition temperature by alloying, good mechanical properties (especially in the case of bulk metallic glasses), negligible magnetic hysteresis, etc. Moreover, the fact that these alloys display negligible magnetic anisotropy fundamentally simplifies the study of

their magnetic transition, making them a good testing ground for analyzing the physics behind the MCE and for developing thermodynamic models to represent their response.

The evolution toward studying TM-based amorphous alloys was gradual. Soft magnetic nanocrystalline alloys of the Finemet (FeSiBCuNb) and Nanoperm (FeZrB) types consist of Fe-rich nanoparticles embedded in a ferromagnetic amorphous matrix and exhibit coercivities of the order of 1 A m^{-1}. When the temperature of the sample is above the Curie temperature of the amorphous matrix, the nanocrystals might behave as superparamagnetic particles (151) or as a system of dipolarly interacting superparamagnetic particles (152, 153).[1] Previous results regarding the MCE of superparamagnetic nanoparticles (154–156) led researchers in the field of soft magnetic nanocrystalline alloys to think that the transition from ferromagnetism (at temperatures below the Curie temperature of the matrix, T_C^{am}) to superparamagnetism (at temperatures above T_C^{am}, high enough to prevent the interactions between the nanocrystals) could give rise to good magnetic refrigerants. Therefore, there were several attempts to study the magnetocaloric response of soft nanocrystalline alloys of the Finemet and Nanoperm families, with different alloying elements to tune T_C^{am} close to room temperature, but results for ΔS_M were less favorable than those for the paradigmatic Gd (157–159). Not only did $|\Delta S_M|$ decrease as the volume fraction of the nanocrystals increased, but also RC did not improve along the nanocrystallization process (148). However, the RC of the amorphous precursor compared favorably with those of other good refrigerant materials (148, 149) such as Fe-doped GdSiGe (12). Subsequently, the magnetocaloric response of most of the well-known families of Fe-based amorphous alloys, with different alloying additives, was studied (150, 160–175), avoiding nanocrystallized samples.

The simplest classification that can be made for amorphous alloys is to divide them between RE-based and TM-based alloys. The first class usually has Curie temperatures well below room temperature and, due to the large magnetic moment of the RE metal (usually Gd), exhibits considerably high magnetic entropy change (176). TM-based amorphous alloys present more modest values, but the transition temperatures can be easily tuned to be close to room temperature or above. At the same time, the economic cost of the constituents of these alloys is usually lower, and they also avoid the inconvenience of corrosion associated with RE metals.

To compare results from different investigations, we extrapolated/interpolated the results quoted in the literature for different values of the applied magnetic field. Studies on the field dependence of magnetocaloric parameters showed that, typically, TM-based amorphous alloys follow $RC \propto H^{1.15}$ (150, 175, 177) and $\Delta S_M^{pk} \propto H^{0.75}$ (165, 177). Therefore, we used those exponents to predict the magnitudes of the alloys' magnetocaloric responses for $\Delta H = 1.5$ T, and the obtained results are presented in **Figure 4** (details of which composition corresponds to each data point are provided in **Supplemental Table 1**). Up to the time of writing, the largest RC_{FWHM} achieved for a TM-based amorphous alloy was 166 J kg^{-1} for $Fe_{88}Zr_7B_4Cu_1$ and $Fe_{82.5}Co_{2.75}Ni_{2.75}Zr_7B_4Cu_1$, with Curie temperatures of 295 K and 398 K, respectively (150). And although these alloys did not exhibit the largest ΔS_M^{pk} (1.32 J kg^{-1} K^{-1} and 1.41 J kg^{-1} K^{-1}, respectively), their values were still close to that of the alloy with the maximum magnetic entropy change, $Fe_{80}Zr_{10}B_{10}$ (1.99 J kg^{-1} K^{-1} for $\Delta H = 1.5$ T) (171). Other alloys from the same $Fe_{88-2x}Co_xNi_xZr_7B_4Cu_1$ family, such as $Fe_{71.5}Co_{8.25}Ni_{8.25}Zr_7B_4Cu_1$, exhibited a ΔS_M^{pk} of 1.95 J kg^{-1} K^{-1} (at the expense of a more reduced RC_{FWHM} of 131 J kg^{-1}). It is worth mentioning that the largest magnetocaloric response in TM-based amorphous alloys was achieved with alloys of the FeZrB type with different

Supplemental Material

[1] Although some authors refer to the magnetic behavior of interacting superparamagnetic particles as superferromagnetism, we prefer to avoid this term because it can be misleading. As opposed to superparamagnetic materials, which exhibit a magnetic response similar to a paramagnet but enhanced due to the large magnetic moments of the nanoparticles, a so-called superferromagnet does not behave as an enhanced ferromagnetic material.

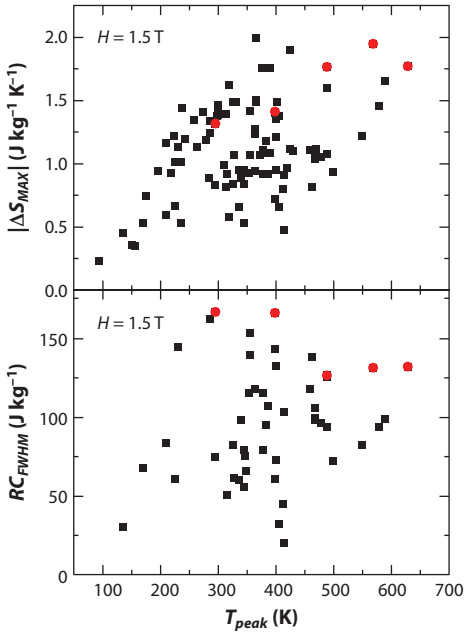

Figure 4

Compilation of the reported magnetocaloric effect of Fe-based amorphous alloys (for studies published through July 2011). Details regarding which composition corresponds to each point may be found in **Supplemental Table 1**. Points marked in red correspond to the series $Fe_{88-2x}Co_xNi_xZr_7B_4Cu_1$.

additions of other alloying elements. And, as would be expected, alloying elements that enhance RC had a deleterious influence on ΔS_M^{pk}; therefore, a balance between both magnitudes should be found.

There is also evidence of a correlation between the magnetic entropy change peak and the average magnetic moment of the alloys (166, 172, 174, 175). Therefore, a strategy for optimizing ΔS_M^{pk} would be to increase the magnetic moment of the alloy without much modification of the Curie temperature, which must remain close to room temperature. Alternatively, the addition of B in the $Fe_{91-x}Mo_8Cu_1B_x$ alloy series allowed tuning of the Curie temperature of the alloys without altering ΔS_M^{pk} (166), which simplifies the design of composite materials for magnetic refrigeration by simplifying the addition of phases in the proper ratio.

RE-based amorphous alloys have applicability for magnetic refrigeration at temperatures in the 50–200 K range (176), depending on the alloying elements. Amorphization enhances the corrosion resistance of such materials, and the addition of other elements, usually cheaper than RE metals, decreases the materials' total cost (178). Both factors enhance the applicability of the alloys. Typical values are $\Delta S_M^{pk} \sim 3.9\,J\,kg^{-1}K^{-1}$ and $RC \sim 150\,J\,kg^{-1}$ for $\Delta H = 1.5$ T (176).

3.4. Multiphase Materials and Composites

The are two main strategies for the optimization of MCMs: (*a*) the design of new alloys and compounds with enhanced performance or (*b*) the use of materials engineering techniques for the optimization of materials that already exist. In the first case, one goal is to increase the magnetic moment, which, provided that the characteristics of the phase transition are maintained, will

cause a larger magnetocaloric response. However, this has to be done without altering the Curie temperature too far from room temperature, which limits the strategies that can be used for achieving the desired result. Therefore, although this is a highly desirable line of research, the expectations of success are limited. Cost reduction is desirable, as is limiting the use of elements that can be extracted only from very few places in the world, because these strategic materials can endanger the ultimate success of any new technology if the geopolitical situation changes. Thus, there is a trade-off between performance and cost. A materials engineering approach can be a complementary line of research with larger certainty of its success. The use of known materials as building blocks for developing composites, nanostructures, graded materials, etc. is already giving promising results, in part due to existing deep knowledge of the material's constituent phases.

Smaïli & Chahine (179) concluded that the ideal material for Ericsson-type magnetic refrigerators should exhibit a constant value of ΔS_M in the temperature range of the operation of the thermodynamic cycle (known as table-like MCE). This can be achieved either by mixing different phases (179–181) or by combining different magnetic phase transitions in the same material (182).

Another property that can be optimized by combining different magnetic phases is RC, as this combination of phases would make the peak broader (at the expense of decreasing the magnitude of the peak). In particular, modeling of the magnetocaloric response of biphasic materials has shown that RC can be enhanced ~90% compared with the starting pure phases, if the appropriate Curie temperatures of the phases are selected and the proper proportion of constituents is used (183). In a biphasic system, the majority phase should have the largest T_C, and the addition of minority phases with a T_C much larger than that of the main phase can decrease to a large extent the RC of the composite as compared with that of the main phase. These results based on numerical calculations have recently been confirmed by experimental measurements on a layered composite (181). Nevertheless, there is still room for improvement of RC using this strategy, as experimental investigations have not yet covered the entire parameter space.

It is worth mentioning that the optimization of the shape of the peak (to obtain a table-like MCE and to broaden the peak to enhance RC) should be done specifically for the magnetic field that will be applied in the refrigerator device, because the optimal proportion of phases changes with field.

3.5. Nanostructured Materials

Studies of the MCE of nanostructured materials are getting more popular in the recent years (184–188). From the applicability point of view, these kinds of materials could be useful for the magnetic refrigeration of electronic chips, microfluidic reactors, and other devices with small dimensions.

Initially, there was evidence that superparamagnetic nanoparticles were better magnetic refrigerants than paramagnetic materials due to their enlarged magnetic moment (154–156). However, their temperatures of application were well below room temperature. For nanocrystalline materials obtained by partial devitrification of an amorphous precursor, as for FeSiBCuNb-type alloys, the nanoparticles' transition to superparamagnetism takes place only above the Curie temperature of the residual amorphous phase (when the interactions between particles vanish) and, therefore, the transition temperature could be tuned to temperatures even above room temperature (153). Although this looked to be a promising way of enhancing the magnetocaloric response of materials for room temperature applications, it was later shown that the appearance of the Fe-rich nanocrystals decreased only RC and ΔS_M^{pk} (148, 169).

In the case of magnetic nanoparticles, MCE is usually not large, but the peak is spread over a larger temperature span (189), which can sometimes increase RC. For materials which present a

FOPT when in bulk form, nanostructuring can lead to a decrease in MCE due to the loss of the first-order character of the phase transition (190). A special case for nanomaterials is the effect associated with surface spin disorder in core-shell nanoparticles, which produces a sizeable MCE (184); being a second-order order-disorder transition, this transition can be studied using the techniques developed for Curie transitions (188).

It has recently been shown that nanostructuring can alter not only the quantitative response of a material, but also its qualitative behavior, which can be completely different from that of its bulk counterpart (185). In the case of arrays of self-organized nanowires, application of magnetic field perpendicular to the wire axis provokes a coexistence of positive and negative MCE, the sign and magnitude of which are controlled by the magnitude of the field. This combination of direct and inverse MCE was previously observed for other bulk materials that undergo several different magnetic transitions (191). However, what is unique in the case of the nanowires is that field-controlled sign of the MCE takes place for a single magnetic transition. This opens new possibilities for the design of completely new applications of the materials.

It is also interesting to point out that the development of multilayers with different compositions of each layer (and therefore with a distribution of Curie temperatures) can be used to enhance the magnetic field responsiveness of MCMs in the H range appropriate for technological applications (192). In such cases, ΔS_M^{pk} has a linear dependence on H in a broad temperature range close to the transition temperature, which is an enhancement with respect to the $H^{0.7}$ behavior typical of bulk materials.

In nanostructured materials, the magnetocaloric response will not only depend on the characteristics of the bulk material (the composition of the phase), but will also be strongly dependent on other factors like particle size (and size distribution), particle concentration, interactions between particles, anisotropy, finite size scaling, etc. Models have been proposed to take into account these effects (185, 186, 193, 194).

4. MODELS OF THE MAGNETOCALORIC EFFECT

To design better MCMs with improved performance, we must understand which of a material's parameters give rise to its magnetocaloric properties and how these parameters can be controlled. Without that understanding, which can be gained through physical models, the search for MCMs would be a process of trial and error based on, at most, educated guesses and plausible ideas. There is also another application for which models of the magnetocaloric response of materials are of crucial importance: refrigerator design. To evaluate the expected performance of such refrigerators when different materials are used, without modeling, engineers would need tables that relate materials properties to the different excitation conditions [e.g., $\Delta S_M(T, H)$], which would generally require very precise experimental measurements. Such measurements would be very time consuming, and the incorporation of those data in the refrigerator's design could be a data-intensive process. However, accurate models of MCMs can replace the tabulated experimental data, simplifying the design process.

4.1. First-Principles Modeling

It has become common to apply first-principles modeling to understand the electronic and magnetic properties of materials with a first-order magnetostructural phase transition (195–198). In this way, exchange coupling energies and magnetic moments can be extracted from the calculations, and subsequently used as inputs in thermomagnetic models, such as the Bean & Rodbell model (199), to extract information about the values of magnetization at finite temperatures,

magnetic entropy, the temperature of the magnetostructural transition, and the MCE. A typical example of the procedure for $Gd_5Si_2Ge_2$ consists of the following steps (197): As this compound exists as an orthorhombic phase at low temperatures, and transforms into a monoclinic one at high temperatures, the total energies and energies of formation in both phases, are calculated to analyze each phase's stability. The magnetic moments of Gd atoms in both phases are subsequently calculated, considering both ferromagnetic and antiferromagnetic alignments of the spins. The magnetic structures are described using exchange coupling between nearest neighbor local moments, with competition between electronic potential energy, which favors ordered magnetism, and electronic kinetic energy, which favors paramagnetism. The exchange coupling energy can be calculated as the difference in total energies of the ferromagnetic and antiferromagnetic types of atomic spin configurations. The calculated values of exchange interaction energies are then introduced in the Heisenberg model to deduce the Curie temperature. Finally, the magnetostructural transition temperature and the MCE are calculated using the Bean & Rodbell model (199), with the parameters obtained from first-principle calculations.

Although good agreement between experimental and calculated parameters can be achieved, the starting point for this kind of modeling requires a deep knowledge of the material under study. Therefore, such techniques are appropriate for explaining observed phenomenology, but their predicting power (before the material is synthesized and measured) is more limited.

Equation of state (EOS): relationship between state variables that provides the state of a system as a function of external stimuli; for a magnetic system and for the purpose of magnetic refrigeration, the most relevant equation of state relates temperature, magnetic field, and magnetization

Critical exponents: for SOPTs at temperatures close to the transition temperature, the exponents that characterize the power law dependencies of the system's magnitudes

4.2. Thermodynamic Models

An alternative to first-principles modeling is a description of the system using thermodynamic models. In such models, the system is described using macroscopic variables, which are obtained by fitting experimental results. There are examples of this kind of procedure for both FOPT (200, 201) and SOPT (202–204) materials.

In the case of materials with hysteresis, such as FOPT materials, even if these phenomenological models can give a description of the effects of hysteresis, the development of microscopic models in which the real magnetic interactions are taken into account (205) is usually helpful for gaining a deeper understanding of the processes involved.

For SOPT materials, thermodynamic models usually deal either with a power expansion of the thermodynamic potential following the formalism of Landau, and therefore consider only mean-field interactions (206), or with an equation of state (EOS), which does not so tightly restrict the temperature and field dependence of magnetization in the environment of the critical temperature. Arrott & Noakes (207) developed an EOS:

$$H^{\frac{1}{\gamma}} = a(T - T_C)M^{\frac{1}{\gamma}} + bM^{\frac{1}{\beta}+\frac{1}{\gamma}}, \qquad 6.$$

where a and b are characteristic parameters of the material under study, and β and γ are the critical exponents. In this way, mean-field behavior need not be imposed; instead, we can control the universality class to which the material pertains by appropriately choosing the values of the critical exponents. By properly manipulating Equation 6, the magnetic entropy change can be expressed as (177)

$$\Delta S_M = -\int_{M_s}^{M_{max}} a\gamma M(a(T - T_C) + bM^{\frac{1}{\beta}})^{\gamma-1} dM. \qquad 7.$$

This means that ΔS_M at each temperature can be obtained from the integration of magnetization data from the spontaneous magnetization, M_S (which corresponds to $H = 0$, taking into account that multidomain configurations are not considered by the EOS; see below) up to M_{max} (which corresponds to the maximum applied field). For the mean-field case, this expression transforms

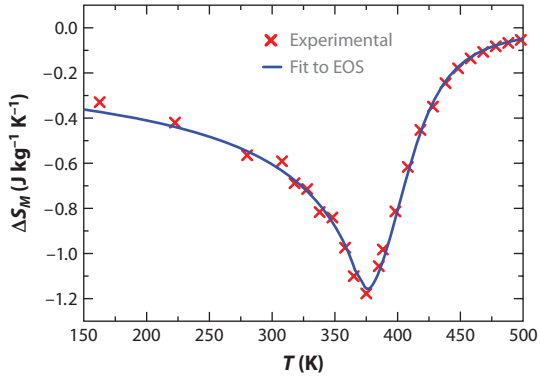

Figure 5

Magnetocaloric effect of the amorphous alloy $Fe_{77}Cr_8B_{15}$ measured up to a maximum field of 1.5 T. Experimental results are red crosses; the blue line is the prediction of the Arrott-Noakes equation of state.

into

$$\Delta S_M(\textit{mean field}) = -\frac{1}{2}a(M^2 - M_s^2). \qquad 8.$$

Therefore, if we determine the critical exponents of the material from the magnetization curves [for example, using the Kouvel-Fisher method (208)] and then fit the magnetization data to Equation 6 to determine the parameters a and b, we are able to reproduce the shape of the magnetic entropy change curves in a relatively broad temperature range (204). As an example, **Figure 5** shows the experimental results for the amorphous alloy $Fe_{77}Cr_8B_{15}$, together with the theoretically predicted values.

When implementing models of a magnetic refrigerator device, it is necessary to introduce the temperature and field dependences of the MCE (209) into the model, usually using mean-field models to describe the thermomagnetic response of the magnetic refrigerant material. These mean-field models lead to certain discrepancies between the predicted and the measured magnetocaloric response, even when the effect of demagnetization is eliminated (210), and those discrepancies can distort the predictions of the efficiency of the refrigerator device. Even if the magnetocaloric peak can be properly reproduced within the experimental error, the shape of the low and high temperature tails might not be properly described. Therefore, it would be more realistic to use models that allow for different critical exponents, which would minimize these difficulties.

The models based on the EOS require that the material reach technical saturation. The EOS relates state functions, which depend on the state of the system and not on the route followed to achieve that state. The spontaneous magnetization of a material is a state function, but the magnetization of a particular sample will depend on how the different domains are configured. Therefore, care must be taken when one is trying to model the magnetic entropy change under small fields.

Even though the most widely used EOS for modeling the MCE is the Arrott-Noakes EOS, there are other predictions that describe material behavior and that do not require an exact knowledge of the EOS that is most appropriate for a particular material. For SOPT materials, we can accept the scaling hypothesis, which is strongly supported by experimental results and theoretical analysis (211), and write the scaling EOS as (212)

$$\frac{H}{M^\delta} = h\left(\frac{t}{M^{1/\beta}}\right), \qquad 9.$$

where $t = (T - T_C)/T_C$ and is the reduced temperature; $h(x)$ is a scaling function; and β and δ are critical exponents that characterize the magnetization behavior along the coexistence curve ($H = 0, t < 0$) and the critical isotherm ($t = 0$), respectively. If we choose the magnetization and magnetic field units in such a way that $h(0) = 1$ and $h(-1) = 0$, the function $h(x)$ is the same for each system in a given universality class.

We can formally invert Equation 9 and introduce it in the Maxwell relation (Equation 2) to rewrite the magnetic entropy change as (213)

$$\Delta S_M / a_M = H^{\frac{1-\alpha}{\Delta}} s(t/H^{1/\Delta}), \qquad 10.$$

where $\Delta = \beta\delta$ is the gap exponent; $s(x)$ is a scaling function; and $a_M = T_C^{-1} A^{\delta+1} B$, with A and B the critical amplitudes at the coexistence curve ($M = A(-t)^{\beta}$) and along the critical isotherm ($H = BM^{\delta}$), respectively (we have made use of the Griffiths equality: $1 - \alpha = \beta + \Delta - 1$). Equation 10 shows that if the reduced temperature t is rescaled by a factor proportional to $H^{1/\Delta}$, and the magnetic entropy change by $a_M H^{(1-\alpha)/\Delta}$, the experimental data should collapse onto a single curve, which has been called universal curve for the MCE (214).

Within this theoretical approach, if we know the EOS that describes a material, and we have the experimental data for a certain value of the field, we can determine the shape of the magnetic entropy change curve for any other field. However, this has limited applications, as we usually do not know a priori the EOS of a newly synthesized material. Recently, a phenomenological procedure was developed to identify the shape of the universal curve for a material without knowing the values of its critical exponents or its EOS (215). An example of the steps followed in this procedure is given in **Figure 6**, for which simulated data for a mean-field model were used. Its construction was based on the assumption that, if such a universal curve exists, equivalent points of the different $\Delta S_M(T)$ curves measured up to different maximum applied fields should collapse onto the same point of the universal curve. Therefore, the key is to identify which are the equivalent points of the different curves for different fields. As there is no doubt that the peaks (which in the mean-field case coincide at T_C) should be in equivalent conditions, we can assume that points that are all at a certain level with respect to the peak are also in equivalent magnetic states (if this hypothesis were not correct, then we would not be able to construct the universal curve). The temperatures of these points, which are marked by crosses in **Figure 6**, are denoted as reference temperatures, T_r, and their identification constitutes the first step of the procedure. The reference temperatures are therefore defined as those which fulfill $\Delta S_M(T_r) = \xi\, \Delta S_M^{pk}$, with a factor $\xi < 1$. The value of ξ is arbitrarily chosen (preferably close to or higher than 1/2) and does not affect the procedure [in **Figure 6**, $\xi = 0.7$ so that $\Delta S_M(T_r) = 0.7\, \Delta S_M^{pk}$]. The second step is the normalization of the curves with respect to their maximum. Finally, the temperature axis is rescaled in such a way that the reference temperatures are all at $\theta = 1$ by using

$$\theta = (T - T_C)/(T_r - T_C). \qquad 11.$$

It is therefore shown that by imposing the position of two points of each of the curves (those at T_C and at T_r), which implies three free parameters, all of the curves collapse onto a single universal curve. In the event that the critical exponents of a material are different from the mean-field case, i.e., the material is from a different universality class, the shape of the curve will be altered. Most notably, the position of the peak will be displaced with respect to T_C. However, using either T_C or the temperature of the peak, T_{pk}, in Equation 11 does not alter the construction of the universal curve (216).

In some cases, like when the effect of the demagnetizing field is important (217) or when there are minority magnetic phases in the material (218), the temperature axis must be rescaled differently below and above T_C, by imposing that the position of the two reference points of each

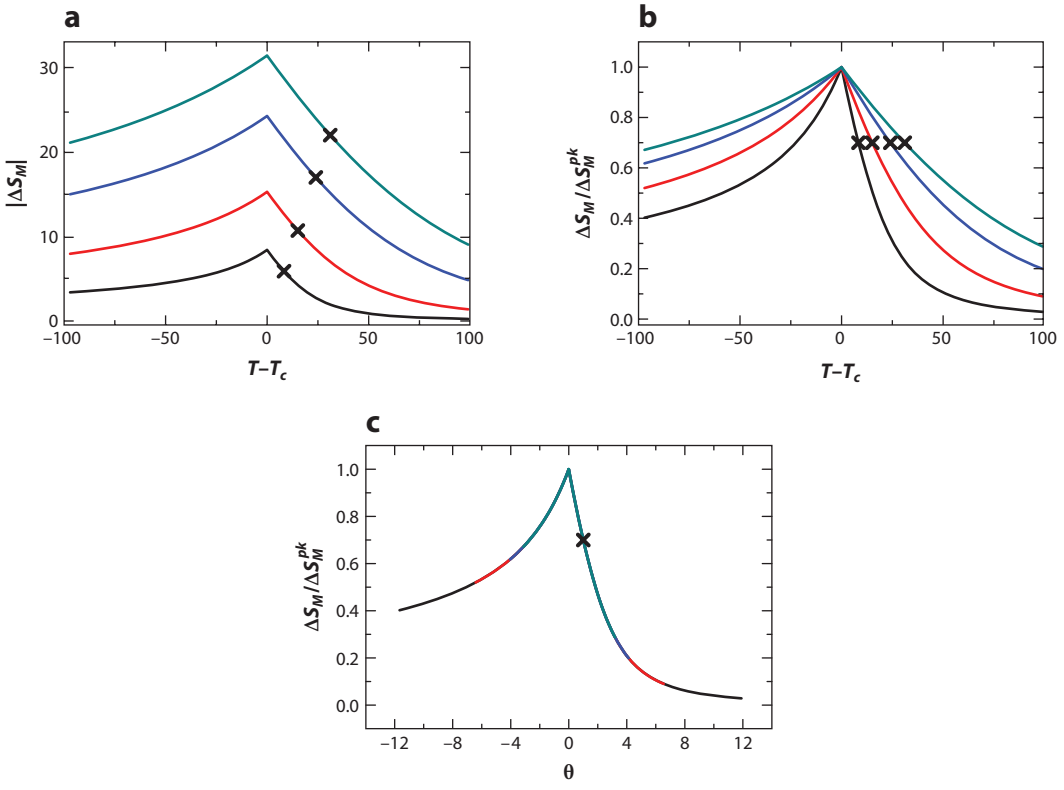

Figure 6

The three steps in the phenomenological construction of the universal curve: (*a*) identification of the reference temperatures (*crosses*), (*b*) normalization, and (*c*) rescaling the temperature axis to place T_r at $\theta = 1$.

curve corresponds to $\theta = \pm 1$. Thus, Equation 11 is replaced by:

$$\theta = \begin{cases} -(T - T_C)/(T_{r1} - T_C); & T \leq T_C \\ (T - T_C)/(T_{r2} - T_C); & T > T_C \end{cases}, \qquad 12.$$

where T_{r1} and T_{r2} are the temperatures of the two reference points of each curve.

This phenomenological construction of the universal curve has been successfully applied to different families of soft magnetic amorphous alloys (165, 215) and lanthanide-based crystalline materials (214, 219), with results fully analogous to those that would be obtained if we were using the theoretical approach described initially (making use of the EOS and the critical exponents of the materials).

Although it seems that the construction of the universal curve is just a theoretical exercise, it has several practical applications for the characterization of materials. For example, once the shape of the curve is known, experimental data can be predicted for fields larger than those measured just by considering that both ΔS_M^{pk} and T_r follow power laws of the field, using exponent values that can be obtained from the experimental $\Delta S_M(T, H)$ curves, and subsequently undoing the aforementioned transformations. Similarly, the universal curve can be used to make extrapolations of data in the temperature axis to ranges where the sample was not measured (166). And for series of alloys with similar values of critical exponents, the universal curve can help predict the MCE

of other alloys within the family, provided that a limited number of experimental points for such alloys are known. From the experimentalist point of view, this technique decreases the noise in the measurements, which allows the resolution of low-field data to be enhanced. For additional examples of these applications, the reader is directed to Reference 177.

This universal behavior can also be extended to the adiabatic temperature change (220) using Equation 1 and taking into account that the specific heat scales with field as

$$\frac{c_p(t, H)}{H^{-\alpha/\Delta}} = c\left(\frac{H}{|t|^{\Delta}}\right), \qquad 13.$$

where c is a scaling function, and the adiabatic temperature change can be expressed as

$$\Delta T_{ad} = H^{\frac{1}{\Delta}} f(t/H^{1/\Delta}), \qquad 14.$$

where f is another scaling function. This equation shows that if the reduced temperature t and the adiabatic temperature change are both rescaled by factors proportional to $H^{1/\Delta}$, the experimental data should collapse onto the same curve. As ΔT_{ad} is a temperature magnitude, it is reasonable that it scales with field in the same way as the temperature axis does. In general, the field dependencies of ΔT_{ad} and ΔS_M are different, which agrees with experimental results (220); however, for the critical exponents of the mean-field model ($\beta = 0.5$; $\gamma = 1$; $\delta = 3$), both field dependencies are the same.

It is important to mention that, although the scaling functions s and f of Equations 10 and 14, respectively, are, in general, different, the phenomenological procedure used to construct the universal curve remains exactly the same, allowing us to overcome the difficulty of knowing the analytical expression of those functions before applying the universal curve for practical purposes.

5. USING THE MAGNETOCALORIC EFFECT TO STUDY MAGNETIC PHASE TRANSITIONS

Early in the study of MCE, the effect was used to gain insight into the nature of phase transitions (22, 23). However, enormous interest later developed in the possible application of MCE for room temperature magnetic refrigeration, and the discovery of the GMCE shifted the focus to the investigation of new MCMs. Nevertheless, MCE can be used as a technique to gain information about the critical exponents of a material or the order of the phase transition, even in cases for which standard techniques do not give accurate results.

Section 4.2 describes how, for materials with a SOPT, ΔS_M and ΔT_{ad} follow a universal behavior in the vicinity of the critical temperature; i.e., when properly rescaled using factors that follow power laws of the field, all the experimental data collapse onto the same curve. Moreover, as RC is simply a combination of the temperature and entropy change axes, it should also scale with field with a power law that has an exponent that is a combination of the exponents associated with ΔS_M and ΔT_{ad} (the definition of RC given by Wood & Potter (11) is an exception to this scaling behavior). Because these scaling powers are combinations of the critical exponents of each material (**Table 1**), it is reasonable to conclude that the critical exponents of the materials can be obtained from the field dependence of their MCE.

In a series of $Gd_5Si_2Ge_{1.9}X_{0.1}$ (with X = Al, Cu, Ga, Mn, Fe, Co) alloys, for those alloys that exhibit a SOPT (X = Al, Cu, Ga, Mn), there is good agreement between the critical exponents obtained using the conventional Kouvel-Fisher method (208) and those obtained from the field dependence of MCE (25). With Fe doping, the appearance of the monoclinic phase is mostly suppressed, and therefore the phase transition is mostly second order, but the Kouvel-Fisher

Table 1 Exponents controlling the field dependence of different magnitudes related to the magnetocaloric effect (*magnitude* $\propto H^{exponent}$)

Magnitude	Exponent
T_r	$1/\Delta$
$T_{pk} - T_C$ (not mean field)	$1/\Delta$
$T_{pk} - T_C$ (mean field)	0
$\Delta S_M (T = T_c)$	$1 + 1/\delta(1 - 1/\beta) = (1 - \alpha)/\Delta$
ΔS_M^{pk}	$1 + 1/\delta(1 - 1/\beta) = (1 - \alpha)/\Delta$
RC_{Area} or RC_{FWHM}	$1 + 1/\delta$

method cannot be applied due to the small contribution of the monoclinic phase. However, scaling the MCE allows the identification of the orthorhombic phase's critical exponents and Curie temperature (the T_C of this phase cannot be experimentally reached for the undoped compound).

These scaling laws for the MCE can also be used to determine the critical properties of a majority phase that coexists with a much higher transition temperature minority phase. Even when the ferromagnetic nature of the minority phase prevents the application of the Kouvel-Fisher method for this purpose, the scaling method is applicable because the high-temperature phase contributes very little to the MCE at the T_C of the majority phase.

Another recent example of using the MCE to analyze the properties of phase transitions is the determination of the order of such transitions using the universal curve for the MCE. As discussed above, the universal curve is applicable only to SOPT materials, and its phenomenological construction rests entirely on magnetic measurements. Through the use of the Banerjee criterion to determine the order of phase transition for the series of cobalt Laves phases $RECo_2$, the transitions for phases containing Pr, Nd, and Dy should be second order, whereas those for phases containing Ho or Er should be first order. However, there is a discrepancy for the case of Dy, which, according to calorimetric data, should be first order. The use of the universal curve allows us to prove, from purely magnetic measurements, that $DyCo_2$ exhibits a FOPT (221) because the transformed ΔS_M curves do not collapse into a single universal curve.

6. CONCLUSIONS AND SUMMARY POINTS

Magnetic refrigeration, based on the MCE, is a promising technology to improve energy efficiency and environmental friendliness. MCMs can be classified according to the order of their phase transition. Those with a FOPT exhibit large magnetic entropy changes, but usually at the expense of magnetic and thermal hysteresis and with a narrow temperature span for operation. SOPT materials have lower magnetic entropy change peaks, but show negligible hysteresis and a broad temperature span, which results in large RCs.

Amorphous alloys based on TM elements can exhibit RCs larger than that of well-known Gd-based crystalline materials with a FOPT. The reduced cost, good mechanical properties, enhanced electrical resistivity, and good corrosion resistance make them interesting subjects of study as magnetic refrigerants.

The MCE of materials with a SOPT can be described using scaling laws. A phenomenological construction of a universal curve, which eliminates field and compositional dependencies, has been proposed and has been experimentally tested for both crystalline and amorphous materials.

Composite materials exhibit enhanced RC with respect to their single-phase constituents only if the proper proportions of phases are selected. These proportions are dependent on the value

of the maximum applied field. The optimal RCs are obtained when the majority phase has the largest Curie temperature of the constituents.

Nanomaterials show magnetocaloric responses that are not only quantitatively but also qualitatively different from those of their bulk counterparts. Therefore, this new behavior can be used to design completely new applications for the materials.

DISCLOSURE STATEMENT

The authors are not aware of any affiliations, memberships, funding, or financial holdings that might be perceived as affecting the objectivity of this review.

ACKNOWLEDGMENTS

The authors acknowledge the financial support of the Spanish Ministry of Science and Innovation and EU FEDER (Project MAT 2010-20537), the PAI of the Regional Government of Andalucía (Project P10-FQM-6462), and the United States Office of Naval Research (Project N00014-11-1-0311).

LITERATURE CITED

1. Warburg E. 1881. Magnetische Untersuchungen. *Ann. Phys.* (*Leipzig*) 13:141–64
2. US Energy Information Administration. 2010. *Annual Energy Review 2009*. Washington, DC: US Gov. Print. Off.
3. Zimm C, Jastrab A, Sternberg A, Pecharsky V, Gschneidner KA Jr, et al. 1998. Description and performance of a near-room temperature refrigerator. In *Advances in Cryogenic Engineering, Vol. 43 Pts. A, B*, ed. P Kittel, pp. 1759–66. New York: Plenum
4. Yu BF, Liu M, Egolf PW, Kitanovski A. 2010. A review of magnetic refrigerator and heat pump prototypes built before the year 2010. *Int. J. Refrig.* 33:1029–60
5. Engelbrecht K, Bahl CRH, Nielsen KK. 2011. Experimental results for a magnetic refrigerator using three different types of magnetocaloric material regenerators. *Int. J. Refrig.* 34:1132–40
6. Tura A, Rowe A. 2011. Permanent magnet magnetic refrigerator design and experimental characterization. *Int. J. Refrig.* 34:628–39
7. Rowe A. 2011. Configuration and performance analysis of magnetic refrigerators. *Int. J. Refrig.* 34:168–77
8. Pecharsky VK, Gschneidner KA Jr. 1999. Magnetocaloric effect from indirect measurements: magnetization and heat capacity. *J. Appl. Phys.* 86:565–75
9. Pecharsky VK, Gschneidner KA Jr, Mudryk Y, Paudyal D. 2009. Making the most of the magnetic and lattice entropy changes. *J. Magn. Magn. Mater.* 321:3541–47
10. Wang GF. 2012. *Magnetic and calorimetric study of magnetocaloric effect in intermetallics exhibiting first-order magnetostructural transitions*. PhD thesis. Univ. Zaragoza
11. Wood ME, Potter WH. 1985. General analysis of magnetic refrigeration and its optimization using a new concept: maximization of refrigerant capacity. *Cryogenics* 25:667–83
12. Provenzano V, Shapiro AJ, Shull RD. 2004. Reduction of hysteresis losses in the magnetic refrigerant $Gd_5Ge_2Si_2$ by the addition of iron. *Nature* 429:853–57
13. Pecharsky VK, Gschneidner KA Jr. 1997. Giant magnetocaloric effect in $Gd_5(Si_2Ge_2)$. *Phys. Rev. Lett.* 78:4494–97
14. Zverev VI, Tishin AM, Kuz'min MD. 2010. The maximum possible magnetocaloric ΔT effect. *J. Appl. Phys.* 107:043907
15. Lyubina J, Schafer R, Martin N, Schultz L, Gutfleisch O. 2010. Novel design of $La(Fe, Si)_{13}$ alloys towards high magnetic refrigeration performance. *Adv. Mater.* 22:3735–39

16. Engelbrecht K, Jensen JB, Bahl CRH. 2012. Experiments on a modular magnetic refrigeration device. *Stroj. Vestn. J. Mech. E* 58:3–8
17. Nielsen KK, Tusek J, Engelbrecht K, Schopfer S, Kitanovski A, et al. 2011. Review on numerical modeling of active magnetic regenerators for room temperature applications. *Int. J. Refrig.* 34:603–16
18. Ujihara M, Carman GP, Lee DG. 2007. Thermal energy harvesting device using ferromagnetic materials. *Appl. Phys. Lett.* 91:093508
19. Love LJ, Jansen JF, McKnight TE, Roh Y, Phelps TJ. 2004. A magnetocaloric pump for microfluidic applications. *IEEE Trans. Nanobiosci.* 3:101–10
20. Palmy C. 2006. A new thermo-magnetic wheel. *Eur. J. Phys.* 27:1289–97
21. Reis MS. 2011. Oscillating magnetocaloric effect. *Appl. Phys. Lett.* 99:052511
22. Belov KP, Nikitin SA, Talalaeva EV, Chernikova LA, Kudryavtseva TV, et al. 1972. Determination of exchange interaction of sublattices in gadolinium iron-garnet on basis of magnetocaloric effect. *Sov. Phys. Jetp USSR* 34:588–92
23. Belov KP, Talalayeva EV, Chernikova LA, Ivanova TI, Ivanovsky VI, Kazakov GV. 1977. Observation of spin reorientation based on measurements of magnetocaloric effect. *Zh. Eksp. Teor. Fiz.* 72:586–91
24. Bonilla CM, Bartolome F, Garcia LM, Parra-Borderias M, Herrero-Albillos J, Franco V. 2010. A new criterion to distinguish the order of magnetic transitions by means of magnetic measurements. *J. Appl. Phys.* 107:09E131
25. Franco V, Conde A, Provenzano V, Shull RD. 2010. Scaling analysis of the magnetocaloric effect in $Gd_5Si_2Ge_{1.9}X_{0.1}$ (X = Al, Cu, Ga, Mn, Fe, Co). *J. Magn. Magn. Mater.* 322:218–23
26. Kuzmin MD, Tishin AM. 1992. Magnetocaloric effect. Part 1: an introduction to various aspects of theory and practice. *Cryogenics* 32:545–58
27. Gschneidner KA Jr, Pecharsky VK. 2000. Magnetocaloric materials. *Annu. Rev. Mater. Sci.* 30:387–429
28. Brück E. 2005. Developments in magnetocaloric refrigeration. *J. Phys. D Appl. Phys.* 38:R381–91
29. Gschneidner KA Jr, Pecharsky VK, Tsokol AO. 2005. Recent developments in magnetocaloric materials. *Rep. Progress Phys.* 68:1479–539
30. Shen BG, Sun JR, Hu FX, Zhang HW, Cheng ZH. 2009. Recent progress in exploring magnetocaloric materials. *Adv. Mater.* 21:4545–64
31. de Oliveira NA, von Ranke PJ. 2010. Theoretical aspects of the magnetocaloric effect. *Phys. Rep.* 489:89–159
32. Dankov SY, Tishin AM, Pecharsky VK, Gschneider KA Jr. 1997. Experimental device for studying the magnetocaloric effect in pulse magnetic fields. *Rev. Sci. Instrum.* 68:2432–37
33. Canepa F, Cirafici S, Napoletano M, Ciccarelli C, Belfortini C. 2005. Direct measurement of the magnetocaloric effect of microstructured Gd eutectic compounds using a new fast automatic device. *Solid State Commun.* 133:241–44
34. Tocado L, Palacios E, Burriel R. 2005. Direct measurement of the magnetocaloric effect in $Tb_5Si_2Ge_2$. *J. Magn. Magn. Mater.* 290:719–22
35. Law JY, Franco V, Ramanujan RV. 2011. Direct magnetocaloric measurements of Fe-B-Cr-X (X = La, Ce) amorphous ribbons. *J. Appl. Phys.* 110:023907
36. Basso V, Kupferling M, Sasso CP, Giudici L. 2008. A Peltier cell calorimeter for the direct measurement of the isothermal entropy change in magnetic materials. *Rev. Sci. Instrum.* 79:063907
37. Tang H, Pecharsky AO, Schlagel DL, Lograsso TA, Pecharsky VK, Gschneidner KA Jr. 2003. Magnetic field induced phase transitions in $Gd_5(Si_{1.95}Ge_{2.05})$ single crystal and the anisotropic magnetocaloric effect. *J. Appl. Phys.* 93:8298–300
38. Wada H, Tanabe Y. 2001. Giant magnetocaloric effect of $MnAs_{1-x}Sb_x$. *Appl. Phys. Lett.* 79:3302–4
39. Zhang HW, Shen J, Dong QY, Zhao TY, Li YX, et al. 2008. The spike in the relation between entropy change and temperature in $LaFe_{11.83}Si_{1.17}$ compound. *J. Magn. Magn. Mater.* 320:1879–83
40. Tocado L, Palacios E, Burriel R. 2009. Entropy determinations and magnetocaloric parameters in systems with first-order transitions: study of MnAs. *J. Appl. Phys.* 105:093918
41. Carvalho AMG, Coelho AA, von Ranke PJ, Alves CS. 2011. The isothermal variation of the entropy (ΔS_T) may be miscalculated from magnetization isotherms in some cases: MnAs and $Gd_5Ge_2Si_2$ compounds as examples. *J. Alloys Compd.* 509:3452–56

42. Kuz'min MD. 2007. Factors limiting the operation frequency of magnetic refrigerators. *Appl. Phys. Lett.* 90:251916
43. Spichkin YI, Zubkov I, Tishin AM, Gschneidner KA Jr, Pecharsky VK. 2009. *Dynamic magnetocaloric effect in the intermetallic R-M (M = Al, Co, Fe) compounds*. Presented at 3rd IIF-IIR Int. Conf. on Magn. Refrig. at Room Temp., Des Moines, Iowa, May 11–15, pp. 139–48
44. Trung NT, Zhang L, Caron L, Buschow KHJ, Brück E. 2010. Giant magnetocaloric effects by tailoring the phase transitions. *Appl. Phys. Lett.* 96:172504
45. Levitin RZ, Snegirev VV, Kopylov AV, Lagutin AS, Gerber A. 1997. Magnetic method of magnetocaloric effect determination in high pulsed magnetic fields. *J. Magn. Magn. Mater.* 170:223–27
46. Medeiros FC, Mello VD, Dantas AL, Sales FHS, Carrico AS. 2011. Giant magnetocaloric effect of thin Ho films. *J. Appl. Phys.* 109:07A914
47. Wohlfarth EP, Rhodes P. 1962. Collective electron metamagnetism. *Philos. Mag.* 7:1817–24
48. Singh NK, Suresh KG, Nigam AK, Malik SK, Coelho AA, Gama S. 2007. Itinerant electron metamagnetism and magnetocaloric effect in RCo_2-based Laves phase compounds. *J. Magn. Magn. Mater.* 317:68–79
49. Khmelevskyi S, Mohn P. 2000. The order of the magnetic phase transitions in RCo_2 (R = rare earth) intermetallic compounds. *J. Phys. Condens. Matter* 12:9453–64
50. Paul-Boncour V, Mazet T. 2009. Investigation of compounds for magnetocaloric applications: $YFe_2H_{4.2}$, $YFe_2D_{4.2}$, and $Y_{0.5}Tb_{0.5}Fe_2D_{4.2}$. *J. Appl. Phys.* 105:013914
51. Zhang Q, Cho JH, Li B, Hu WJ, Zhang ZD. 2009. Magnetocaloric effect in Ho_2In over a wide temperature range. *Appl. Phys. Lett.* 94:182501
52. Chen J, Shen BG, Dong QY, Hu FX, Sun JR. 2010. Giant reversible magnetocaloric effect in metamagnetic HoCuSi compound. *Appl. Phys. Lett.* 96:152501
53. Hu FX, Shen BG, Sun JR, Cheng ZH, Rao GH, Zhang XX. 2001. Influence of negative lattice expansion and metamagnetic transition on magnetic entropy change in the compound $LaFe_{11.4}Si_{1.6}$. *Appl. Phys. Lett.* 78:3675–77
54. Jia L, Sun JR, Shen J, Dong QY, Zou JD, et al. 2009. Magnetocaloric effects in the $La(Fe,Si)_{13}$ intermetallics doped by different elements. *J. Appl. Phys.* 105:07A924
55. Yan A, Muller KH, Gutfleisch O. 2005. Structure and magnetic entropy change of melt-spun $LaFe_{11.57}Si_{1.43}$ ribbons. *J. Appl. Phys.* 97:036102
56. Liu XB, Liu XD, Altounian Z. 2005. Phase formation and magnetocaloric effect in rapidly quenched $La(Fe_{1-x}Co_x)_{11.4}Si_{1.6}$. *J. Appl. Phys.* 98:113904
57. Lyubina J, Gutfleisch O, Kuz'min MD, Richter M. 2009. $La(Fe,Si)_{13}$-based magnetic refrigerants obtained by novel processing routes. *J. Magn. Magn. Mater.* 321:3571–77
58. Hu FX, Shen BG, Sun JR, Cheng ZH, Zhang XX. 2000. Magnetic entropy change in $La(Fe_{0.98}Co_{0.02})_{11.7}Al_{1.3}$. *J. Phys. Condens. Matter* 12:L691–96
59. Pecharsky VK, Gschneidner KA Jr. 1997. Tunable magnetic regenerator alloys with a giant magnetocaloric effect for magnetic refrigeration from ~20 to ~290 K. *Appl. Phys. Lett.* 70:3299–301
60. Shull RD, Provenzano V, Shapiro AJ, Fu A, Lufaso MW, et al. 2006. The effects of small metal additions (Co, Cu, Ga, Mn, Al, Bi, Sn) on the magnetocaloric properties of the $Gd_5Ge_2Si_2$ alloy. *J. Appl. Phys.* 99:08K908
61. Li JQ, Sun WA, Jian YX, Zhuang YH, Huang WD, Liang JK. 2006. The giant magnetocaloric effect of $Gd_5Si_{1.95}Ge_{2.05}$ enhanced by Sn doping. *J. Appl. Phys.* 100:073904
62. Provenzano V, Zhang TB, Shapiro A, Chen YG, Shull RD. 2008. Magnetocaloric properties and structure of the $Gd_5Ge_{1.8}Si_{1.8}Sn_{0.4}$ compound. *IEEE Trans. Magnet.* 44:3048–51
63. Yuzuak E, Dincer I, Elerman Y. 2010. Magnetocaloric properties of the $Gd_5Si_{2.05-x}Ge_{1.95-x}Mn_{2x}$ compounds. *J. Rare Earths* 28:477–80
64. Yüzüak E, Dincer I, Elerman Y. 2010. Giant magnetocaloric effect in the $Gd_5Ge_{2.025}Si_{1.925}In_{0.05}$ compound. *Chin. Phys. B* 19:037502
65. Podmiljsak B, McGuiness P, Miklavic B, Rozman KZ, Kobe S. 2009. Magnetocaloric properties and nanoscale structure of Fe-doped $Gd_5Ge_2Si_2$ alloys. *J. Appl. Phys.* 105:07A941
66. Prabahar K, Kumar DMR, Raja MM, Palit M, Chandrasekaran V. 2010. Solidification behaviour and microstructural correlations in magnetocaloric Gd-Si-Ge-Nb alloys. *Mater. Sci. Eng. B* 172:294–99

67. Pecharsky AO, Gschneidner KA Jr, Pecharsky VK. 2003. The giant magnetocaloric effect of optimally prepared $Gd_5Si_2Ge_2$. *J. Appl. Phys.* 93:4722–28
68. Yan A, Handstein A, Kerschl P, Nenkov K, Muller KH, Gutfleisch O. 2004. Effect of composition and cooling rate on the structure and magnetic entropy change in $Gd_5Si_xGe_{4-x}$. *J. Appl. Phys.* 95:7064–66
69. Gschneidner KA Jr, Pecharsky VK. 1999. Magnetic refrigeration materials (invited). *J. Appl. Phys.* 85:5365–68
70. Prabahar K, Kumar DMR, Raja MM, Chandrasekaran V. 2011. Phase analysis and magnetocaloric properties of Zr substituted Gd-Si-Ge alloys. *J. Magn. Magn. Mater.* 323:1755–59
71. Phan M, Yu S. 2007. Review of the magnetocaloric effect in manganite materials. *J. Magn. Magn. Mater.* 308:325–40
72. Dörr K. 2006. Ferromagnetic manganites: spin-polarized conduction versus competing interactions. *J. Phys. D Appl. Phys.* 39:R125–50
73. Morelli DT, Mance AM, Mantese JV, Micheli AL. 1996. Magnetocaloric properties of doped lanthanum manganite film. *J. Appl. Phys.* 79:373
74. Zhang XX, Tejada J, Xin Y, Sun GF, Wong KW, Bohigas X. 1996. Magnetocaloric effect in $La_{0.67}Ca_{0.33}MnO_\delta$ and $La_{0.60}Y_{0.07}Ca_{0.33}MnO_\delta$ bulk materials. *Appl. Phys. Lett.* 69:3596
75. Zhang T, Fang YZ, Dressel M, Wang XP, Fang QF. 2010. Nanometer size effect on the structure and magnetic properties of high oxygen content ferromagnetic $PrMnO_{3+\delta}$ nanoparticles. *J. Appl. Phys.* 108:113901
76. Pekala M, Drozd V, Fagnard JF, Vanderbemden P. 2010. Magnetocaloric effect in nano- and polycrystalline manganites $La_{0.5}Ca_{0.5}MnO_3$. *J. Alloys Compd.* 507:350–55
77. Tang W, Lu WJ, Luo X, Wang BS, Zhu XB, et al. 2010. Size-induced changes of structural, magnetic and magnetocaloric properties of $La_{0.7}Ca_{0.2}Ba_{0.1}MnO_3$. *Phys. B: Condens. Matter* 405:2733–41
78. Hao C, Zhao B, Huang Y, Kuang G, Sun Y. 2011. A-site-disorder-dependent magnetocaloric properties in the mono-valent-metal doped $La_{0.7}Ca_{0.3}MnO_3$ manganites. *J. Alloys Compd.* 509:5877–81
79. Ji Q, Lv B, Wang PF, Cai HL, Wu XS, et al. 2009. Effects of *A*-site cation disorder on structure and magnetocaloric properties in Y and Sr codoped $La_{2/3}Ca_{1/3}MnO_3$ compounds. *J. Appl. Phys.* 105:07D713
80. Amaral J, Tavares P, Reis M, Araujo J, Mendonca T, et al. 2008. The effect of chemical distribution on the magnetocaloric effect: a case study in second-order phase transition manganites. *J. Non-Cryst. Solids* 354:5301–3
81. Ekber Irmak A, Coskun A, Tasarkuyu E, Akturk S, Unlu G, et al. 2010. The influence of the sintering temperature on the structural and the magnetic properties of doped manganites: $La_{0.95}Ag_{0.05}MnO_3$ and $La_{0.75}Ag_{0.25}MnO_3$. *J. Magn. Magn. Mater.* 322:945–51
82. Othmani S, Bejar M, Dhahri E, Hlil EK. 2009. The effect of the annealing temperature on the structural and magnetic properties of the manganites compounds. *J. Alloys Compd.* 475:46–50
83. Szymczak R, Kolano R, Kolano-Burian A, Pietosa J, Szymczak H. 2010. Cooling by adiabatic pressure application in $La_{0.7}Ca_{0.3}MnO_3$ magnetocaloric effect material. *J. Magn. Magn. Mater.* 322:1589–91
84. Brück E, Tegus O, Camthanh D, Trung N, Buschow K. 2008. A review on Mn based materials for magnetic refrigeration: structure and properties. *Int. J. Refrig.* 31:763–70
85. Mandal K, Yan A, Kerschl P, Handstein A, Gutfleisch O, Muller KH. 2004. The study of magnetocaloric effect in R_2Fe_{17} (R = Y, Pr) alloys. *J. Phys. D Appl. Phys.* 37:2628–31
86. Gorria P, Álvarez P, Marcos JS, Sánchez Llamazares JL, Pérez MJ, Blanco JA. 2009. Crystal structure, magnetocaloric effect and magnetovolume anomalies in nanostructured Pr_2Fe_{17}. *Acta Mater.* 57:1724–33
87. Pawlik K, Skorvanek I, Kovac J, Pawlik P, Wyslocki JJ, Bodak OI. 2006. Phase structure and magnetocaloric effect in binary Pr-Fe alloys. *J. Magn. Magn. Mater.* 304:E510–12
88. Álvarez P, Gorria P, Sánchez Llamazares JL, Pérez MJ, Franco V, et al. 2011. Magnetic properties and magneto-caloric effect in pseudo-binary intermetallic $(Ce,R)_2Fe_{17}$ compounds (R = Y, Pr and Dy). *Intermetallics* 19:982–87
89. Kuchin AG, Iwasieczko W. 2011. Magnetocaloric effect in the $Ce_2Fe_{17-x}Mn_x$ helical magnets. *J. Alloys Compd.* 509:6763–67
90. Fang YK, Chang CW, Yeh CC, Chang HW, Li W, Chang WC. 2008. Microstructure and magnetocaloric effect of melt-spun Y_2Fe_{17} ribbons. *J. Appl. Phys.* 103:07B302

91. Banerjee D, Kumar P, Suresh KG, Nigam AK. 2007. Anomalous magnetic and magnetocaloric properties of Er_2Ni_{17}. *J. Phys. D Appl. Phys.* 40:2691–94
92. Kuchin AG, Iwasieczko W. 2010. Enhancement of the magnetocaloric effect in the $Lu_2Fe_{17-x}Mn_x$ system. *Solid State Commun.* 150:1580–83
93. Tripathy SK, Suresh KG, Nigam AK. 2006. A comparative study of the magnetocaloric effect in Gd_3Co and Gd_3Ni. *J. Magn. Magn. Mater.* 306:24–29
94. Kumar P, Suresh KG, Nigam AK. 2011. Magnetothermal effect in Gd_3Rh. *J. Appl. Phys.* 109:07A909
95. Li B, Du J, Ren WJ, Hu WJ, Zhang Q, et al. 2008. Large reversible magnetocaloric effect in Tb_3Co compound. *Appl. Phys. Lett.* 92:242504
96. Shen J, Wu JF, Sun JR. 2009. Room-temperature large refrigerant capacity of $Gd_6Co_2Si_3$. *J. Appl. Phys.* 106:083902
97. Zhang CL, Wang DH, Han ZD, Tang SL, Gu BX, Du YW. 2006. Large magnetic entropy changes in $NdFe_{12}B_6$ compound. *Appl. Phys. Lett.* 89:122503
98. Huang YJ, Shi ZL, Zhang CL, Li SZ, Chen N, et al. 2008. Structural properties and Mössbauer spectra of metastable $NdFe_{12}B_6$. *Mater. Lett.* 62:85–87
99. Wang F, Shen BG, Zhang J, Sun JR, Meng FB, Li YX. 2010. Magnetic properties and magnetocaloric effect in compound $PrFe_{12}B_6$. *Chin. Phys. B* 19:067501
100. Hu F-x, Shen B-g, Sun J-r, Wu G-h. 2001. Large magnetic entropy change in a Heusler alloy $Ni_{56.2}Mn_{23.1}Ga_{24.3}$ single crystal. *Phys. Rev. B* 64:132412
101. Ingale B, Gopalan R, Raja MM, Chandrasekaran V, Ram S. 2007. Magnetostructural transformation, microstructure, and magnetocaloric effect in Ni-Mn-Ga Heusler alloys. *J. Appl. Phys.* 102:013906
102. Marcos J, Planes A, Mañosa L, Casanova F, Batlle X, et al. 2002. Magnetic field induced entropy change and magnetoelasticity in Ni-Mn-Ga alloys. *Phys. Rev. B* 66:224413
103. Marcos J, Manosa L, Planes A, Casanova F, Batlle X, Labarta A. 2003. Multiscale origin of the magnetocaloric effect in Ni-Mn-Ga shape-memory alloys. *Phys. Rev. B* 68:094401
104. Krenke T, Duman E, Acet M, Wassermann EF, Moya X, et al. 2005. Inverse magnetocaloric effect in ferromagnetic Ni-Mn-Sn alloys. *Nat. Mater.* 4:450–54
105. Khovaylo VV, Skokov KP, Gutfleisch O, Miki H, Takagi T, et al. 2010. Peculiarities of the magnetocaloric properties in Ni-Mn-Sn ferromagnetic shape memory alloys. *Phys. Rev. B* 81:214406
106. Han ZD, Wang DH, Zhang CL, Xuan HC, Gu BX, Du YW. 2007. Low-field inverse magnetocaloric effect in $Ni_{50-x}Mn_{39+x}Sn_{11}$ Heusler alloys. *Appl. Phys. Lett.* 90:042507
107. Kainuma R, Imano Y, Ito W, Sutou Y, Morito H, et al. 2006. Magnetic-field-induced shape recovery by reverse phase transformation. *Nature* 439:957–60
108. Shamberger PJ, Ohuchi FS. 2009. Hysteresis of the martensitic phase transition in magnetocaloric-effect Ni-Mn-Sn alloys. *Phys. Rev. B* 79:144407
109. Hernando B, Llamazares JLS, Santos JD, Prida VM, Baldomir D, et al. 2008. Magnetocaloric effect in melt spun $Ni_{50.3}Mn_{35.5}Sn_{14.4}$ ribbons. *Appl. Phys. Lett.* 92:132507
110. Babita I, Gopalan R, Ram S, Fecht HJ. 2009. A large inverse magnetocaloric effect in $Ni_{49.0}Mn_{37.4}Sn_{13.6}$ melt-spun ribbons at room temperature. *Nanosci. Nanotechnol. Lett.* 1:151–55
111. Babita I, Ram S, Gopalan R, Chandrasekaran V. 2009. Dynamic inverse-magnetocaloric and martensite transition in $Ni_{49}Mn_{38}Sn_{13}$ nanocrystals in low magnetic fields. *Philos. Mag. Lett.* 89:399–407
112. Pathak AK, Khan M, Dubenko I, Stadler S, Ali N. 2007. Large magnetic entropy change in $Ni_{50}Mn_{50-x}In_x$ Heusler alloys. *Appl. Phys. Lett.* 90:262504
113. Pasquale M, Sasso CP, Lewis LH, Giudici L, Lograsso T, Schlagel D. 2005. Magnetostructural transition and magnetocaloric effect in $Ni_{55}Mn_{20}Ga_{25}$ single crystals. *Phys. Rev. B* 72:094435
114. Khovaylo VV, Skokov KP, Koshkid'ko YS, Koledov VV, Shavrov VG, et al. 2008. Adiabatic temperature change at first-order magnetic phase transitions: $Ni_{2.19}Mn_{0.81}Ga$ as a case study. *Phys. Rev. B* 78:060403
115. Moya X, Manosa L, Planes A. 2007. Cooling and heating by adiabatic magnetization in the $Ni_{50}Mn_{34}In_{16}$ magnetic shape-memory alloy. *Phys. Rev. B* 75:184412
116. Aliev AM, Batdalov AB, Kamilov IK, Koledov VV, Shavrov VG, et al. 2010. Magnetocaloric effect in ribbon samples of Heusler alloys Ni-Mn-M (M = In, Sn). *Appl. Phys. Lett.* 97:212505
117. Lin S, Tegus O, Brück E, Dagula W, Gortenmulder TJ, Buschow KHJ. 2006. Structural and magnetic properties of $MnFe_{1-x}Co_xGe$ compounds. *IEEE Trans. Magnet.* 42:3776–78

118. Zhang CL, Wang DH, Cao QQ, Han ZD, Xuan HC, Du YW. 2009. Large magnetic entropy change and broad working temperature span in $CoMnSi_{0.88}Ge_{0.12}$ alloy. *J. Phys. D Appl. Phys.* 42:015007
119. Songlin S, Dagula W, Tegus O, Brück E, Klaasse JCP, et al. 2002. Magnetic phase transition and magnetocaloric effect in $Mn_{5-x}Fe_xSi_3$. *J. Alloys Compd.* 334:249–52
120. Songlin S, Dagula W, Tegus O, Brück E, de Boer FR, Buschow KHJ. 2010. Magnetic and magnetocaloric properties of $Mn_5Ge_{3-x}Sb_x$. *J. Alloys Compd.* 337:269–71
121. Xie ZG, Geng DY, Zhang ZD. 2010. Reversible room-temperature magnetocaloric effect in Mn_5PB_2. *Appl. Phys. Lett.* 97:202504
122. Morikawa T, Wada H, Kogure R, Hirosawa S. 2004. Effect of concentration deviation from stoichiometry on the magnetism of MnAsSb. *J. Magn. Magn. Mater.* 283:322–28
123. Wada H, Matsuo S, Mitsuda A. 2009. Pressure dependence of magnetic entropy change and magnetic transition in $MnAs_{1-x}Sb_x$. *Phys. Rev. B* 79:092407
124. de Campos A, Rocco DL, Carvalho AM, Caron L, Coelho AA, et al. 2006. Ambient pressure colossal magnetocaloric effect tuned by composition in $Mn_{1-x}Fe_xAs$. *Nat. Mater.* 5:802–4
125. Amaral JS, Amaral VS. 2009. The effect of magnetic irreversibility on estimating the magnetocaloric effect from magnetization measurements. *Appl. Phys. Lett.* 94:042506
126. Cui WB, Liu W, Liu XH, Guo S, Han Z, et al. 2009. Magnetocaloric effects and reduced thermal hysteresis in Si-doped MnAs compounds. *J. Alloys Compd.* 479:189–92
127. Cui WB, Lv XK, Yang F, Yu Y, Skomski R, et al. 2010. Interstitial-nitrogen effect on phase transition and magnetocaloric effect in Mn(As,Si) (invited). *J. Appl. Phys.* 107:09A938
128. Tegus O, Brück E, Buschow KHJ, de Boer FR. 2002. Transition-metal-based magnetic refrigerants for room-temperature applications. *Nature* 415:150–52
129. Gribanov IF, Golovchan AV, Varyukhin DV, Val'kov VI, Kamenev VI, et al. 2009. Magnetic and magnetocaloric properties of the alloys $Mn_{2-x}Fe_xP_{0.5}As_{0.5}$ ($0 <= x <= 0.5$). *Low Temp. Phys.* 35:786–91
130. Cam Thanh DT, Brück E, Tegus O, Klaasse JCP, Gortenmulder TJ, Buschow KHJ. 2006. Magnetocaloric effect in MnFe(P,Si,Ge) compounds. *J. Appl. Phys.* 99:08Q107
131. Wang DM, Song L, Wang YH, Zhang W, Bilige Q, Tegus O. 2011. Magnetocaloric effect in $MnFeP_{0.63}Ge_{0.12}Si_{0.25}B_x$ ($x = 0, 0.01, 0.02, 0.03$) compounds. *Acta Metall. Sin.* 47:344–48
132. Song L, Wang GF, Ou ZQ, Haschaolu O, Tegus O, et al. 2009. Magnetic properties and magnetocaloric effect of $MnFeP_{0.5}Ge_{0.5-x}Si_x$ compounds. *J. Alloys Compd.* 474:388–90
133. Cam Thanh DT, Brück E, Trung NT, Klaasse JCP, Buschow KHJ, et al. 2008. Structure, magnetism, and magnetocaloric properties of $MnFeP_{1-x}Si_x$ compounds. *J. Appl. Phys.* 103:07B318
134. Trung NT, Ou ZQ, Gortenmulder TJ, Tegus O, Buschow KHJ, Brück E. 2009. Tunable thermal hysteresis in MnFe(P,Ge) compounds. *Appl. Phys. Lett.* 94:102513
135. Annaorazov MP, Asatryan KA, Myalikgulyev G, Nikitin SA, Tishin AM, Tyurin AL. 1992. Alloys of the Fe-Rh system as a new class of working material for magnetic refrigerators. *Cryogenics* 32:872
136. Gschneidner KA Jr, Pecharsky VK. 2000. Magnetocaloric materials. *Annu. Rev. Mater. Sci.* 30:387–429
137. Manekar M, Roy SB. 2008. Reproducible room temperature giant magnetocaloric effect in Fe-Rh. *J. Phys. D Appl. Phys.* 41:192004
138. Sandratskii L, Mavropoulos P. 2011. Magnetic excitations and femtomagnetism of FeRh: a first-principles study. *Phys. Rev. B* 83:174408
139. Manekar M, Roy SB. 2011. Very large refrigerant capacity at room temperature with reproducible magnetocaloric effect in $Fe_{0.975}Ni_{0.025}Rh$. *J. Phys. D Appl. Phys.* 44:242001
140. Rong CB, Liu JP. 2007. Temperature- and magnetic-field-induced phase transitions in Fe-rich FePt alloys. *Appl. Phys. Lett.* 90:222504
141. Gass J, Srikanth H, Kislov N, Srinivasan SS, Emirov Y. 2008. Magnetization and magnetocaloric effect in ball-milled zinc ferrite powder. *J. Appl. Phys.* 103:07B309
142. Gopalan EV, Al-Omari IA, Kumar DS, Yoshida Y, Joy PA, Anantharaman MR. 2010. Inverse magnetocaloric effect in sol-gel derived nanosized cobalt ferrite. *Appl. Phys. A Mater. Sci. Process.* 99:497–503
143. Tohei T, Wada H, Kanomata T. 2003. Negative magnetocaloric effect at the antiferromagnetic to ferromagnetic transition of Mn_3GaC. *J. Appl. Phys.* 94:1800–2

144. Wang BS, Tong P, Sun YP, Zhu XB, Luo X, et al. 2009. Reversible room-temperature magnetocaloric effect with large temperature span in antiperovskite compounds $Ga_{1-x}CMn_{3+x}$ ($x = 0$, 0.06, 0.07, and 0.08). *J. Appl. Phys.* 105:083907
145. Maeda H, Sato M, Uehara M. 1983. Fe-Zr amorphous alloys for magnetic refrigerants near room temperature. *J. Jpn. Inst. Met.* 47:688–91
146. Belova VM, Stolyarov VL. 1984. Temperature-dependence of magnetocaloric effect in amorphous ferromagnets. *Fiz. Tverd. Tela* 26:851–53
147. Foldeaki M, Giguere A, Gopal BR, Chahine R, Bose TK, et al. 1997. Composition dependence of magnetic properties in amorphous rare-earth-metal-based alloys. *J. Magn. Magn. Mater.* 174:295–308
148. Franco V, Blázquez JS, Conde CF, Conde A. 2006. A Finemet-type alloy as a low-cost candidate for high-temperature magnetic refrigeration. *Appl. Phys. Lett.* 88:042505
149. Johnson F, Shull RD. 2006. Amorphous-FeCoCrZrB ferromagnets for use as high-temperature magnetic refrigerants. *J. Appl. Phys.* 99:08K909
150. Caballero-Flores R, Franco V, Conde A, Knipling KE, Willard MA. 2010. Influence of Co and Ni addition on the magnetocaloric effect in $Fe_{88-2x}Co_xNi_xZr_7B_4Cu_1$ soft magnetic amorphous alloys. *Appl. Phys. Lett.* 96:182506
151. Slawska-Waniewska A, Gutowski M, Lachowicz HK, Kulik T, Matyja H. 1992. Superparamagnetism in a nanocrystalline Fe-based metallic-glass. *Phys. Rev. B* 46:14594–97
152. Franco V, Conde CF, Conde A, Kiss LF. 2005. Relationship between coercivity and magnetic moment of superparamagnetic particles with dipolar interaction. *Phys. Rev. B* 72:174424
153. Franco V, Kiss LF, Kemeny T, Vincze I, Conde CF, Conde A. 2002. High-temperature evolution of coercivity in nanocrystalline alloys. *Phys. Rev. B* 66:224418
154. McMichael RD, Shull RD, Swartzendruber LJ, Bennett LH, Watson RE. 1992. Magnetocaloric effect in superparamagnets. *J. Magn. Magn. Mater.* 111:29–33
155. Bennett LH, McMichael RD, Swartzendruber LJ, Shull RD, Watson RE. 1992. Monte Carlo and mean-field calculations of the magnetocaloric effect of ferromagnetically interacting clusters. *J. Magn. Magn. Mater.* 104–7:1094–95
156. Belova VM, Nikolaev VI, Stuchebn.Vm. 1973. Magnetocaloric effect in superparamagnetic substances. *Zh. Eksp. Teor. Fiz.* 64:1746–49
157. Didukh P, Ślawska-Waniewska A. 2003. Magnetocaloric effect in slightly crystallised Co-Nb-Cu-Si-B alloy. *J. Magn. Magn. Mater.* 254–55:407–9
158. Skorvanek I, Kovac J. 2004. Magnetocaloric behaviour in amorphous and nanocrystalline FeNbB soft magnetic alloys. *Czech. J. Phys.* 54:D189–92
159. Atalay S, Gencer H, Kolat VS. 2005. Magnetic entropy change in $Fe_{74-x}Cr_xCu_1Nb_3Si_{13}B_9$ ($x = 14$ and 17) amorphous alloys. *J. Non-Cryst. Solids* 351:2373–77
160. Min SG, Kim KS, Yu SC, Suh HS, Lee SW. 2005. Analysis of magnetization and magnetocaloric effect in amorphous FeZrMn ribbons. *J. Appl. Phys.* 97:10M310
161. Franco V, Blázquez JS, Conde A. 2006. The influence of Co addition on the magnetocaloric effect of Nanoperm-type amorphous alloys. *J. Appl. Phys.* 100:064307
162. Franco V, Borrego JM, Conde A, Roth S. 2006. Influence of Co addition on the magnetocaloric effect of FeCoSiAlGaPCB amorphous alloys. *Appl. Phys. Lett.* 88:132509
163. Franco V, Borrego JM, Conde CF, Conde A, Stoica M, Roth S. 2006. Refrigerant capacity of FeCrMoCuGaPCB amorphous alloys. *J. Appl. Phys.* 100:083903
164. Kim KS, Min SG, Yu SC, Oh SK, Kim YC, Kim KY. 2006. The large magnetocaloric effect in amorphous $Fe_{91-x}Y_xZr_9$ ($x = 0$, 5, 10) alloys. *J. Magn. Magn. Mater.* 304:E642–44
165. Franco V, Blázquez JS, Millan M, Borrego JM, Conde CF, Conde A. 2007. The magnetocaloric effect in soft magnetic amorphous alloys. *J. Appl. Phys.* 101:09C503
166. Franco V, Conde CF, Blázquez JS, Conde A, Svec P, et al. 2007. A constant magnetocaloric response in FeMoCuB amorphous alloys with different Fe/B ratios. *J. Appl. Phys.* 101:093903
167. Franco V, Conde CF, Conde A, Kiss LF. 2007. Enhanced magnetocaloric response in Cr/Mo containing Nanoperm-type amorphous alloys. *Appl. Phys. Lett.* 90:052509
168. Min SG, Kim KS, Yu SC, Kim YC, Kim KY, et al. 2007. The magnetic entropy change on amorphous FeMnZr alloys. *J. Magn. Magn. Mater.* 310:2820–22

169. Skorvanek I, Kovac J, Marcin J, Svec P, Janickovic D. 2007. Magnetocaloric effect in amorphous and nanocrystalline $Fe_{81-x}Cr_xNb_7B_{12}$ ($x = 0$ and 3.5) alloys. *Mater. Sci. Eng. A* 449–51:460–63
170. Torrens-Serra J, Roth S, Rodriguez-Viejo J, Clavaguera-Mora MT. 2008. Effect of Nb in the nanocrystallization and magnetic properties of FeNbBCu amorphous alloys. *J. Non-Cryst. Solids* 354:5110–12
171. Fang YK, Yeh CC, Hsieh CC, Chang CW, Chang HW, et al. 2009. Magnetocaloric effect in Fe-Zr-B-M (M = Mn, Cr, and Co) amorphous systems. *J. Appl. Phys.* 105:07A910
172. Wang YY, Bi XF. 2009. The role of Zr and B in room temperature magnetic entropy change of FeZrB amorphous alloys. *Appl. Phys. Lett.* 95:262501
173. Alvarez P, Gorria P, Marcos JS, Barquin LF, Blanco JA. 2010. The role of boron on the magneto-caloric effect of FeZrB metallic glasses. *Intermetallics* 18:2464–67
174. Caballero-Flores R, Franco V, Conde A, Kiss LF. 2010. Influence of Mn on the magnetocaloric effect of nanoperm-type alloys. *J. Appl. Phys.* 108:073921
175. Law JY, Ramanujan RV, Franco V. 2010. Tunable Curie temperatures in Gd alloyed Fe-B-Cr magnetocaloric materials. *J. Alloys Compd.* 508:14–19
176. Wang WH. 2009. Bulk metallic glasses with functional physical properties. *Adv. Mater.* 21:4524–44
177. Franco V, Conde A. 2010. Scaling laws for the magnetocaloric effect in second order phase transitions: from physics to applications for the characterization of materials. *Int. J. Refrig.* 33:465–73
178. Mayer C, Gorsse S, Ballon G, Caballero-Flores R, Franco V, Chevalier B. 2011. Tunable magnetocaloric effect in Gd-based glassy ribbons. *J. Appl. Phys.* 110:053920
179. Smaïli A, Chahine R. 1997. Composite materials for Ericsson-like magnetic refrigeration cycle. *J. Appl. Phys.* 81:824–29
180. Chaturvedi A, Stefanoski S, Phan MH, Nolas GS, Srikanth H. 2011. Table-like magnetocaloric effect and enhanced refrigerant capacity in $Eu_8Ga_{16}Ge_{30}$-EuO composite materials. *Appl. Phys. Lett.* 99:162513
181. Paticopoulos SC, Caballero-Flores R, Franco V, Blázquez JS, Conde A, et al. 2012. Enhancement of the magnetocaloric effect in composites: experimental validation. *Solid State Commun*. In press; doi: 10.1016/j.ssc.2012.05.015
182. de Oliveira IG, von Ranke PJ, Nobrega EP. 2003. Understanding the table-like magnetocaloric effect. *J. Magn. Magn. Mater.* 261:112–17
183. Caballero-Flores R, Franco V, Conde A, Knipling KE, Willard MA. 2011. Optimization of the refrigerant capacity in multiphase magnetocaloric materials. *Appl. Phys. Lett.* 98:102505
184. Poddar P, Srinath S, Gass J, Prasad BLV, Srikanth H. 2007. Magnetic transition and large magnetocaloric effect associated with surface spin disorder in Co and CocoreAgshell nanoparticles. *J. Phys. Chem. C* 111:14060–66
185. Franco V, Pirota KR, Prida VM, Neto A, Conde A, et al. 2008. Tailoring of magnetocaloric response in nanostructured materials: role of anisotropy. *Phys. Rev. B* 77:104434
186. Skomski R, Binek C, Mukherjee T, Sahoo S, Sellmyer DJ. 2008. Temperature- and field-induced entropy changes in nanomagnets. *J. Appl. Phys.* 103:07B329
187. Mukherjee T, Sahoo S, Skomski R, Sellmyer DJ, Binek C. 2009. Magnetocaloric properties of Co/Cr superlattices. *Phys. Rev. B* 79:144406
188. Franco V, Conde A, Sidhaye D, Prasad BLV, Poddar P, et al. 2010. Field dependence of the magnetocaloric effect in core-shell nanoparticles. *J. Appl. Phys.* 107:09A902
189. Poddar P, Gass J, Rebar DJ, Srinath S, Srikanth H, et al. 2006. Magnetocaloric effect in ferrite nanoparticles. *J. Magn. Magn. Mater.* 307:227–31
190. Hueso LE, Sande P, Miguens DR, Rivas J, Rivadulla F, Lopez-Quintela MA. 2002. Tuning of the magnetocaloric effect in $La_{0.67}Ca_{0.33}MnO_{3-\delta}$ nanoparticles synthesized by sol-gel techniques. *J. Appl. Phys.* 91:9943–47
191. Wang DH, Zhang CL, Xuan HC, Han ZD, Zhang JR, et al. 2007. The study of low-field positive and negative magnetic entropy changes in $Ni_{43}Mn_{46-x}Cu_xSn_{11}$ alloys. *J. Appl. Phys.* 102:013909
192. Caballero-Flores R, Franco V, Conde A, Kiss LF, Peter L, Bakonyi I. 2012. Magnetic multilayers as a way to increase the magnetic field responsiveness of magnetocaloric materials. *J. Nanosci. Nanotechnol.* In press
193. Baldomir D, Rivas J, Serantes D, Pereiro M, Arias JE, et al. 2007. Magnetocaloric effects in magnetic nanoparticle systems: a Monte Carlo study. *J. Non-Cryst. Solids* 353:790–92

194. Serantes D, Baldomir D, Pereiro M, Hernando B, Prida VM, et al. 2009. Magnetocaloric effect in dipolar chains of magnetic nanoparticles with collinear anisotropy axes. *Phys. Rev. B* 80:134421
195. Harmon BN, Antonov VN. 2002. Electronic structure, optical, and magneto-optical properties of $Gd_5(Si_2Ge_2)$ compound. *J. Appl. Phys.* 91:9815–20
196. Mihalik M, Vejpravova J, Rusz J, Divis M, Svoboda P, Sechovsky V. 2004. Anisotropic magnetic properties and specific-heat study of a $TbFe_2Si_2$ single crystal. *Phys. Rev. B* 70:134405
197. Paudyal D, Pecharsky VK, Gschneidner KA Jr, Harmon BN. 2006. Electron correlation effects on the magnetostructural transition and magnetocaloric effect in $Gd_5Si_2Ge_2$. *Phys. Rev. B* 73:144406
198. Buchelnikov VD, Sokolovskiy VV, Herper HC, Ebert H, Gruner ME, et al. 2010. First-principles and Monte Carlo study of magnetostructural transition and magnetocaloric properties of $Ni2+xMn1-xGa$. *Phys. Rev. B* 81:094411
199. Bean C, Rodbell D. 1962. Magnetic disorder as a first-order phase transformation. *Phys. Rev.* 126:104–15
200. Basso V, Bertotti G, LoBue M, Sasso CP. 2005. Theoretical approach to the magnetocaloric effect with hysteresis. *J. Magn. Magn. Mater.* 290:654–57
201. Spichkin YI, Tishin AM. 2005. Thermodynamic model of the magnetocaloric effect near the first-order magnetic phase transitions. *J. Magn. Magn. Mater.* 290:700–2
202. Oesterreicher H, Parker FT. 1984. Magnetic cooling near Curie temperatures above 300 K. *J. Appl. Phys.* 55:4334–38
203. Romanov AY, Silin VP. 1997. On magnetocalorical effect of heterogeneous ferromagnets. *Fiz. Met. Metalloved.* 83:5–11
204. Franco V, Conde A, Kiss LF. 2008. Magnetocaloric response of FeCrB amorphous alloys: predicting the magnetic entropy change from the Arrott-Noakes equation of state. *J. Appl. Phys.* 104:033903
205. Santana RP, de Oliveira NA, von Ranke PJ. 2011. Magnetocaloric properties of compounds with first order phase transition: hysteresis effect. *J. Alloys Compd.* 509:6346–49
206. Kuz'min MD. 2008. Landau-type parametrization of the equation of state of a ferromagnet. *Phys. Rev. B* 77:184431
207. Arrott A, Noakes JE. 1967. Approximate equation of state for nickel near its critical temperature. *Phys. Rev. Lett.* 19:786–89
208. Kouvel JS, Fisher ME. 1964. Detailed magnetic behavior of nickel near its Curie point. *Phys. Rev.* 136:A1626–32
209. Nielsen KK, Bahl CRH, Smith A, Pryds N, Hattel J. 2010. A comprehensive parameter study of an active magnetic regenerator using a 2D numerical model. *Int. J. Refrig.* 33:753–64
210. Bahl CRH, Nielsen KK. 2009. The effect of demagnetization on the magnetocaloric properties of gadolinium. *J. Appl. Phys.* 105:013916
211. Stanley HE. 1999. Scaling, universality, and renormalization: three pillars of modern critical phenomena. *Rev. Mod. Phys.* 71:S358–66
212. Widom B. 1965. Equation of state in the neighborhood of the critical point. *J. Chem. Phys.* 43:3898–905
213. Franco V, Conde A, Romero-Enrique JM, Blázquez JS. 2008. A universal curve for the magnetocaloric effect: an analysis based on scaling relations. *J. Phys. Condens. Matter* 20:285207
214. Franco V, Conde A, Pecharsky VK, Gschneidner KA Jr. 2007. Field dependence of the magnetocaloric effect in Gd and $(Er_{1-x}Dy_x)Al_2$: Does a universal curve exist? *EPL* 79:47009
215. Franco V, Blázquez JS, Conde A. 2006. Field dependence of the magnetocaloric effect in materials with a second order phase transition: a master curve for the magnetic entropy change. *Appl. Phys. Lett.* 89:222512
216. Franco V, Conde A, Kuz'min MD, Romero-Enrique JM. 2009. The magnetocaloric effect in materials with a second order phase transition: Are T_C and T peak necessarily coincident? *J. Appl. Phys.* 105:07A917
217. Caballero-Flores R, Franco V, Conde A, Kiss LF. 2009. Influence of the demagnetizing field on the determination of the magnetocaloric effect from magnetization curves. *J. Appl. Phys.* 105:07A919
218. Franco V, Caballero-Flores R, Conde A, Dong QY, Zhang HW. 2009. The influence of a minority magnetic phase on the field dependence of the magnetocaloric effect. *J. Magn. Magn. Mater.* 321:1115–20
219. Dong QY, Zhang HW, Sun JR, Shen BG, Franco V. 2008. A phenomenological fitting curve for the magnetocaloric effect of materials with a second-order phase transition. *J. Appl. Phys.* 103:116101

220. Franco V, Conde A, Romero-Enrique JM, Spichkin YI, Zverev VI, Tishin AM. 2009. Field dependence of the adiabatic temperature change in second order phase transition materials: application to Gd. *J. Appl. Phys.* 106:103911
221. Bonilla CM, Herrero-Albillos J, Bartolome F, Garcia LM, Parra-Borderias M, Franco V. 2010 . Universal behavior for magnetic entropy change in magnetocaloric materials: an analysis on the nature of phase transitions. *Phys. Rev. B* 81:224424

Annual Review of
Materials Research

Volume 42, 2012

Contents

Index

Errata

An online log of corrections to *Annual Review of Materials Research* articles may be found at http://matsci.annualreviews.org/errata.shtml